A Density Functional Theory Study of CO_2 Interaction

with Brookite TiO_2

by

Monique M. Rodriguez

A Thesis Presented in Partial Fulfillment
of the Requirements for the Degree
Master of Science

Approved July 2012 by the
Graduate Supervisory Committee:

Jean M. Andino, Chair
David R. Nielsen
Lenore Dai

ARIZONA STATE UNIVERSITY

July 2012

ABSTRACT

Over the past years, an interest has arisen in resolving two major issues: increased carbon dioxide (CO_2) emissions and depleting energy resources. A convenient solution would be a process that could simultaneously use CO_2 while producing energy. The photocatalytic reduction of CO_2 to fuels over the photocatalyst titanium dioxide (TiO_2) is such a process. However, this process is presently inefficient and unsuitable for industrial applications. A step toward making this process more effective is to alter TiO_2 based photocatalysts to improve their activity.

The interactions of CO_2 with oxygen-deficient and unmodified (210) surfaces of brookite TiO_2 were studied using first-principle calculations on cluster systems. Charge and spin density analyses were implemented to determine if charge transfer to the CO_2 molecule occurred and whether this charge transfer was comparable to that seen with the oxygen-deficient and unmodified anatase TiO_2 (101) surfaces. Although the unmodified brookite (210) surface provided energetically similar CO_2 interactions as compared to the unmodified anatase (101) surface, the unmodified brookite surface had negligible charge transfer to the CO_2 molecule. This result suggests that unmodified brookite is not a suitable catalyst for the reduction of CO_2. However, the results also suggest that modification of the brookite surface through the creation of oxygen vacancies may lead to enhancements in CO_2 reduction. The computational results were supported with laboratory data for CO_2 interaction with perfect brookite and oxygen-deficient brookite. The laboratory data, generated using diffuse

i

reflectance Fourier transform infrared spectroscopy, confirms the presence of CO_2^- on only the oxygen-deficient brookite.

Additional computational work was performed on I-doped anatase (101) and I-doped brookite (210) surface clusters. Adsorption energies and charge and spin density analyses were performed and the results compared. While charge and spin density analyses showed minute charge transfer to CO_2, the calculated adsorption energies demonstrated an increased affinity for CO_2 adsorption onto the I-doped brookite surface. Gathering the results from all calculations, the computational work on oxygen-deficient, I-doped, and unmodified anatase and brookite surface structures suggest that brookite TiO_2 is a potential photocatalysts for CO_2 photoreduction.

TABLE OF CONTENTS

LIST OF TABLES

LIST OF FIGURES

LIST OF SYMBOLS

Chapter 1

INTRODUCTION

      With increasing greenhouse gas emissions and depleting energy resources, interest has arisen in the development of environmentally clean and safe processes that are capable of expanding our energy infrastructure. Because carbon dioxide (CO_2) has been identified as a significant greenhouse gas, it is critical to find methods for removing this compound from the atmosphere. Carbon capture and sequestration in geological formations is a current option for removing CO_2, but uncertainties exist regarding permanent storage of the CO_2 (White *et al.* 2003). A promising solution that could simultaneously utilize CO_2 and produce potential fuel products is the photocatalytic reduction of CO_2 in the presence of water vapor.

      The reduction of CO_2 is a challenging reaction because of the inertness and stability of the compound. In order to achieve CO_2 reduction, most methods require high energy inputs to achieve high-temperatures and pressures (Usubharatana *et al.* 2006). Table 1 lists some of the processes available for CO_2 reduction to fuels. Among them, the photocatalytic reduction of CO_2 by means of light energy activation is of great interest.

Table 1: CO_2 conversion to fuel processes (Centi *et al.* 2009)

Technology	Products	Advantages	Challenges
Dry Reforming of Methane	Carbon monoxide C_2 hydrocarbons, hydrogen	Suitable conversion efficiency	High energy input, catalyst coking (deactivation)
Electrochemical Reduction	Carbon monoxide, formic acid, methane	Energy efficient, direct or indirect conversion, inexpensive	Mass transport limitations, short-term stability of catalyst and electrode material
Hydrogenation	Carbon monoxide, ethanol, formic acid, methane, methanol	Suitable conversion efficiency	Intensive use of resources, catalyst coking (deactivation)
Photocatalytic Reduction	Carbon monoxide, formic acid, formaldehyde, methane, methanol	Direct conversion, inexpensive	Low yields, limited visible light use

The photoreduction of CO_2 uses mild conditions (room temperature and low pressure) and lower energy inputs. Since light energy is required for activation, the potential use of solar energy would provide a free, continuous and readily available power supply. Concurrent with lowering the direct emissions of CO_2 to the atmosphere, the photoreduction of CO_2 also has the potential to produce valuable chemicals and fuel products. This latter aspect makes the photocatalytic reduction approach attractive as compared to other CO_2 removal methods.

Photocatalysis

A photoinduced reaction accelerated by the presence of a catalyst is known as photocatalysis. The catalyst, or photocatalyst, is often times a

semiconductor. Semiconductor photocatalysts promote chemical reactions upon light irradiation. Semiconductors have an energy void region called the band gap. The band gap of a semiconductor extends from the top of the filled valance band (VB) to the bottom of the vacant conduction band (CB). Upon light activation at energy levels equivalent to the band gap energy, electron-hole pairs are generate which are essential for a reaction. Hindering the recombination of the electron-hole pair provides enough time for charge transfer to occur on the surface of the semiconductor, thereby allowing the chemical reaction to proceed.

A chemical reaction in a heterogeneous photocatalytic system occurs at the semiconductor's surface. For this research, heterogeneous refers to a gas-solid particle system. The reaction is initiated by photon energy absorption that is equal to or greater than the band gap energy of the semiconductor. Upon light absorption, electrons are excited from the valence band to the conduction band, leaving behind holes in the valance band. The dotted circle in Figure 1 depicts electron excitation by light energy from the valence band to the conduction band resulting in electron-hole pair generation in the semiconductor. These electron-hole pairs can follow several pathways that affect the product formation.
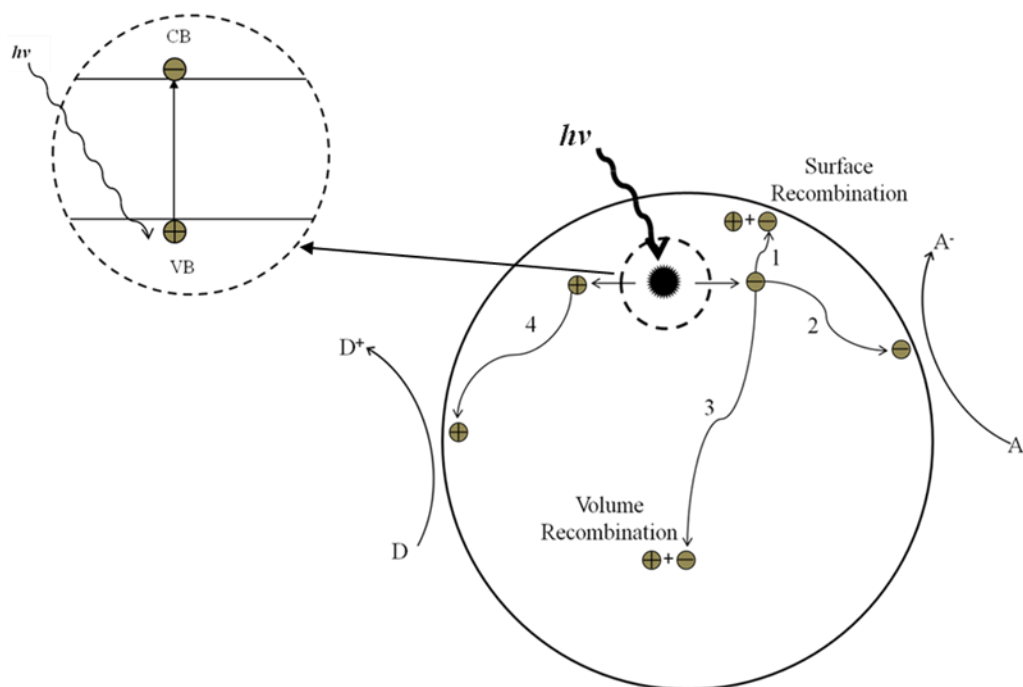
Figure 1: Photoexcitation schematic in a semiconductor (Linsebigler *et al.* 1995)

Figure 1 depicts the possible photoexcitation pathways in a semiconductor. Once the electron is excited to the conduction band, leaving behind the hole in the valance band, the electrons and holes can recombine within the volume of the semiconductor or migrate to the surface where they can either recombine or react with adsorbed species. Pathways 1 and 3 demonstrate electron-hole recombination at the surface and in the volume, respectively. Pathway 2 demonstrates electron donation to reduce an electron acceptor species (A) while pathway 4 shows a hole combining with an electron from a donor species (D).

Electron-hole recombination is a common problem in photocatalytic reactions. Recombination of the electron-hole pair is an undesirable event in photocatalysis because it competes with charge transfer to the reactants that are

4

adsorbed to the semiconductor's surface, consequently competing with product formation. This competition determines the product outcome and affects the efficiency of the photocatalyst. The lifetime of an electron-hole pair is in the nanosecond range (Linsebigler *et al.* 1995). Extending this lifetime would thereby slow electron-hole recombination, making the process more efficient. The photocatalytic reaction rate heavily depends on the type of semiconductor used as the photocatalyst and the initiating light radiation (Koci *et al.* 2008).

A photocatalytic semiconductor must have a redox potential of the photogenerated valence band hole that is positive enough for the hole to act as an accepter while the redox potential of the photogenerated conduction band electron must be negative enough for the electron to act as a donor. The semiconductor must be resistant to photocorrosion and toxic by-product formation as well as commercially and economically available. Titanium dioxide (TiO_2) has been the photocatalyst of choice in several processes because it meets these criteria for multiple applications.

Titanium Dioxide (TiO_2)

TiO_2 has been widely used for industrial applications because of its photoactivity, stability, low cost, and non-toxicity. TiO_2 is a wide band gap photocatalyst, with an average band gap energy of 3.2 eV. This large band gap catalyst requires high energy activation in the ultraviolet (UV) light region. Only 2-3% of the sunlight reaching the earth is in the UV region (Kitano *et al.* 2007). TiO_2 exists in three naturally occurring crystallographic forms: rutile, anatase, and

brookite (see Figure 2). The rutile and anatase phases have a tetragonal crystal

structure while the brookite phase has an orthorhombic crystal structure. Each

phase has a designated band gap: rutile, 3.00 eV (Henderson 2011); anatase, 3.20

eV (Henderson 2011); and brookite, 3.29-3.40 eV (Di Paola *et al.* 2008; Koelsch

et al. 2002). Because of the past difficulties in synthesizing pure samples of

brookite, a definitive band gap value has not been established.
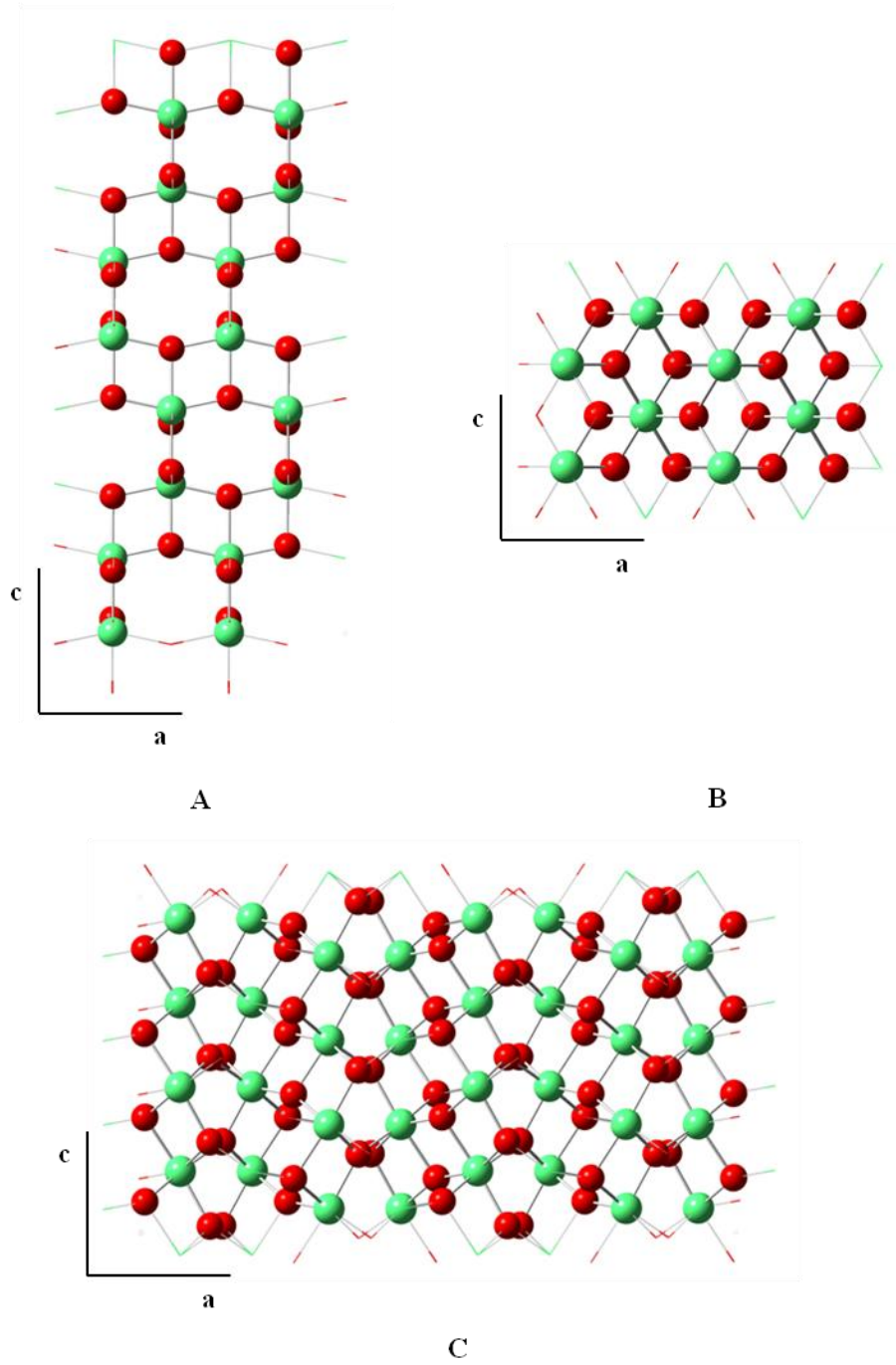
Figure 2: Crystallographic forms of TiO_2; anatase (A), rutile (B), and brookite

(C). Atoms represented according to color: Ti in green and O in red.

The rutile and anatase phases are the more extensively studied of the three phases. Rutile is widely used in the pigments and cosmetic industry (Li *et al.* 2007). Because anatase is regarded as the more photocatalytically active of the two phases (Hurum *et al.* 2003), it is commonly used for photocatalytic purposes (Li *et al.* 2007). The rutile phase is considered less active since it has lower surface affinity for several organic compounds and has higher recombination rates of photogenerated charge pairs (Hurum *et al.* 2006). However, the rutile phase can be excited by wavelengths that extend into the visible light range (410nm) whereas the excitation wavelength for anatase is in the UV region (385nm) (Hurum *et al.* 2003). The brookite phase is the least studied, partly due to past difficulties in creating pure brookite samples (Addamo *et al.* 2006; Dambournet *et al.* 2010; Park *et al.* 2009; Kandiel *et al.* 2010; Xie *et al.* 2009).

Two main concerns exist with TiO_2 as a photocatalyst: the wide band gap requires high energy input in the UV region and the fast charge recombination rate decreases its efficiency. By modifying TiO_2, a potential exists for shifting the required energy input from the UV region to the visible light region and reducing the charge recombination rates. Utilizing mixed-phase TiO_2 or modification of the TiO_2 through deposition and doping of the surface are some of the possible TiO_2 modifications that can have positive effects on the photoefficiency of the catalyst.

Mixed-Phase TiO$_2$

Utilizing mixed-phase TiO$_2$ is a topic of interest, particularly anatase-rutile mixtures, due to its increased photoactivity. Anatase-rutile mixed-phase TiO$_2$, the standard being commercially available Degussa-Evonik P25, has higher photoactivity than either pure rutile or pure anatase (Hurum *et al.* 2003; Agrios *et al.* 2003; Henderson 2011). Degussa P25 has a composition of ~25% rutile and ~75% anatase. The increased activity of anatase-rutile mixtures is a combination of different effects.

Because the rutile phase has a smaller band gap energy and can be activated in the visible light range, lower light energy input can be used to activate anatase-rutile TiO$_2$ catalysts. Additionally, electron transfer from the rutile phase to the anatase phase results in a decreased electron-hole recombination due to electron trapping sites in anatase.

Electron trapping sites are defect sites in a semiconductor that capture electrons. These can be in the lattice, at the particles surface or distortions at an interface. Hurum *et al.* (2006) identified anatase surface trapping sites and interfacial sites in P25, and demonstrated that distorted interface promotes electron transfer. Because the anatase trapping site is lower in energy than both the anatase and rutile conduction band, the electron migrates from the rutile CB to the anatase trapping site. This stabilizes charge transfer. Figure 3 depicts electron transfer in an anatase-rutile mixed-phase TiO$_2$ catalyst.
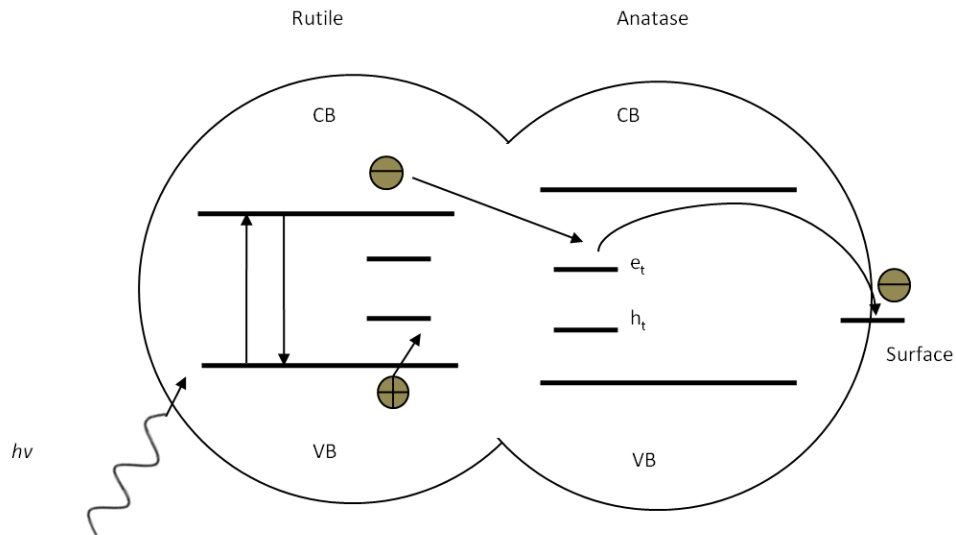
Figure 3: Electron transfer in a light-activated anatase-rutile TiO_2 mixture. 'e_t' and 'h_t' represent the electron trapping site and hole trapping site, respectively.

Deposition and Doped TiO_2

Depositing metals (e.g. copper, silver, or gold) on the surface of TiO_2 can help inhibit the electron-hole pair recombination rate by acting as charge-carrier trappers (Linsebigler *et al.* 1995; Li *et al.* 2010; Koci *et al.* 2008). These trapped charges can then quickly transfer to adsorbed reactants (Tseng *et al.* 2004; Song *et al.* 1999). Doping TiO_2 with metals or non-metals can also increase the photocatalytic activity of the catalyst by shifting the wavelength region that is needed for activation of the catalyst from the UV to the visible region, thus allowing catalytic activation by solar radiation (Chai *et al.* 2011).

Doping creates impurity bands or band gap states in the band gap which can aid in electron-hole pair generation because lower energy inputs are required to activate the catalyst (Koci *et al.* 2010; Lopez *et al.* 2009). Figure 4

10

demonstrates metal deposition onto a TiO_2 surface and impurity band states in the band gap that are created by doping.
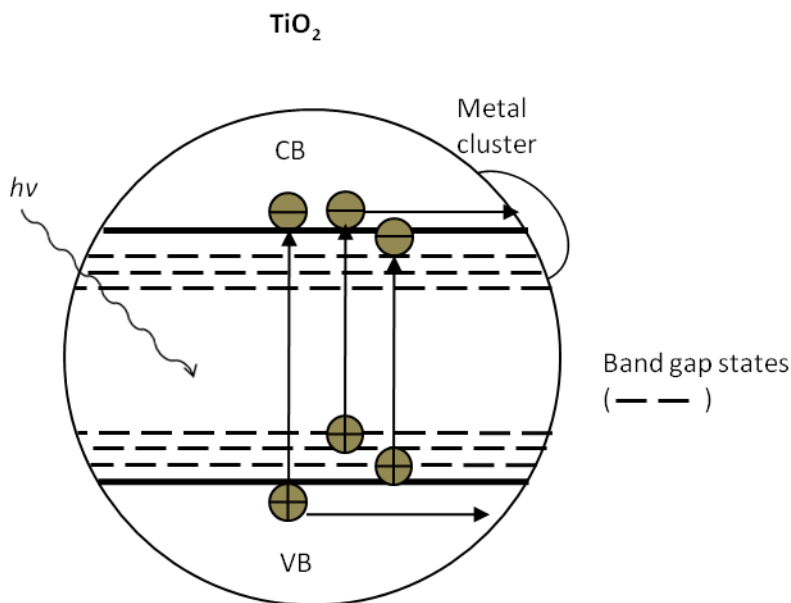
Figure 4: Metal deposition and impurity band states (in dashed line) in band gap region due to doping in TiO_2.

Photocatalytic Reduction of CO_2 over TiO_2

For the reduction of CO_2 by water to occur, TiO_2 must absorb light energy that is equal to or greater than its band gap energy. Upon light absorption, electrons (e^-) are excited from the valence band (VB) to the conduction band (CB), leaving behind holes (h^+) in the valance band (Eq. 1). The electrons and holes migrate to the surface of the TiO_2 catalyst where the electrons are hypothesized to react with adsorbed CO_2 to form carbon dioxide radicals ($^{\cdot}CO_2^-$) (Eq. 2) and the holes react with adsorbed water to form H^+ and oxygen (Eq. 3).

11

These three steps are important for the photoreduction of CO_2 to proceed, and are essential for product formation (Centi *et al.* 2009; Koci *et al.* 2008).

$$TiO_2 \rightarrow e^- + h^+ \qquad\qquad \text{Eq. 1}$$

$$CO_{2\ (adsorbed)} + e^- \rightarrow \cdot CO_{2\ (adsorbed)}^- \qquad\qquad \text{Eq. 2}$$

$$2H_2O_{adsorbed} + 4h^+ \rightarrow 4H^+ + O_2 \qquad\qquad \text{Eq. 3}$$
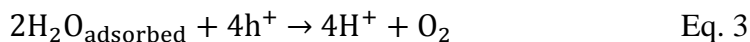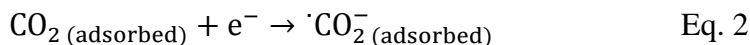
Subsequent reactions can occur that can result in several potential products. Figure 5 depicts the activation of TiO_2 by light and the generated electron-hole pair reacting with CO_2 and water to possibly produce useful products, such as methane and methanol.
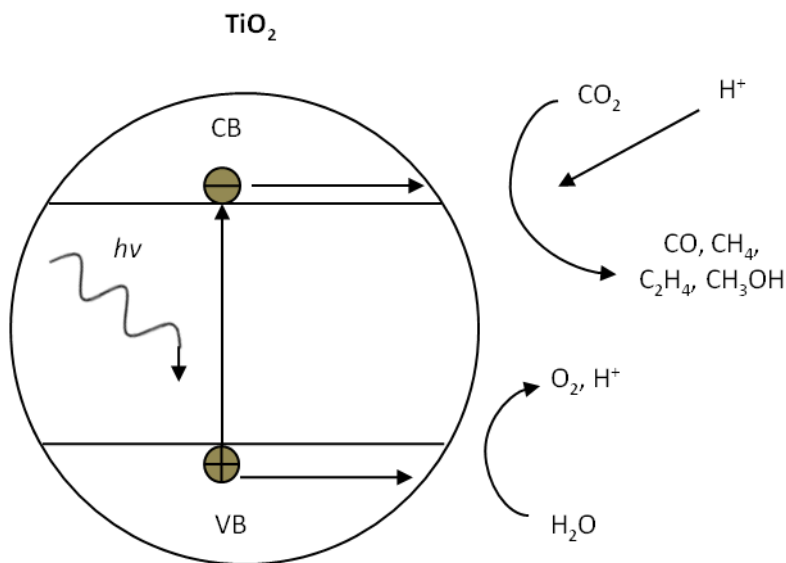
Figure 5: Reaction schematic for CO_2 reduction

In recent years researchers have investigated the photocatalytic reduction of CO_2 over various modified and unmodified forms of TiO_2 (Linsebigler *et al.* 1995; Anpo *et al.* 1995; Tseng *et al.* 2004; Kitano *et al.* 2007; Koci *et al.* 2008;

Varghese *et al.* 2010; Yang *et al.* 2009; Indrakanti *et al.* 2009; Li *et al.* 2010; Koci *et al.* 2010; He *et al.* 2010). When examining the CO_2 reduction process, only rutile, anatase and rutile-anatase mixtures have been explored, either as pure phase components or with metal and non-metal modifications to the anatase or rutile materials (Li *et al.* 2010; Tseng *et al.* 2004; Yang *et al.* 2009). However, the CO_2 conversion efficiency to useful products currently is rather low for industrial applications with specific rates ranging from less than 1 μmol CO_2 converted/g-TiO_2/h to about 25 μmol CO_2 converted/g-TiO_2/h (Indrakanti *et al.* 2009). In order for the photocatalytic reduction of CO_2 to be an economically viable process, the specific rates would have to significantly increase to ~10s of mmol CO_2 converted/g-TiO_2/h under visible light irradiation (Indrakanti *et al.* 2009).

It is thought that the formation of the CO_2^- on the surface of TiO_2 upon light irradiation is the first step (Centi *et al.* 2009), and experimental evidence demonstrates the existence of the CO_2^- on irradiated TiO_2 (Rasko *et al.* 1994). He *et al.* (2010) performed first-principle calculations on cluster and periodic models of the anatase TiO_2 (101) surface, the most exposed anatase surface, to determine the binding configurations of CO_2. The results of their research show CO_2^- formation on the surface of anatase TiO_2.

As stated previously, CO_2 reduction over rutile, anatase, and mixtures of these two phases have been performed. No research had previously been published concerning CO_2 reduction over brookite TiO_2. However, recent studies have suggested that brookite is a good photocatalyst and may exhibit even higher

13

photocatalytic activity than both rutile and anatase (Park *et al.* 2009; Li *et al.* 2008; Pan *et al.* 2009). Specifically, density functional theory (DFT) calculations performed on the brookite (210) and anatase (101) surfaces demonstrated that the brookite (210) surface has similar structural building blocks as the anatase (101) surface (Li *et al.* 2008). Both the anatase (101) and brookite (210) surfaces have blocks consisting of exposed 5- and 6-coordinated Ti atoms and 2- and 3- coordinated O atoms. The brookite surface has slightly shorter interatomic distances and a different block arrangement (Li *et al.* 2008). These features assisted in the generation of highly active sites and stronger adsorptions of water and formic acid, typical probe molecules, on the brookite surface (Li *et al.* 2008).

Because the brookite phase has not been previously explored for CO_2 photoreduction, yet the literature suggests that this phase has increased photocatalytic activity, it is of keen interest to see how CO_2 interacts with this TiO_2 polymorph. The purpose of this work was to use computational chemistry to investigate the interaction of CO_2 and the formation of CO_2^- on the brookite (210) surface. Ultimately the goal was to determine whether the brookite (210) surface could more readily facilitate charge transfer to CO_2 as compared to the anatase TiO_2 (101) surface. Enhancing the charge transfer to surface adsorbed species could ultimately result in enhanced product production rates, thus increasing the utility of the CO_2 photoreduction process for energy generation. The brookite (210) surface was chosen because it is one of the most frequently exposed and stable surfaces of the brookite phase with similar structural features to the anatase

14

(101) surface (Gong and Selloni 2007). Additional work was performed on the oxygen-deficient brookite (210) surface.

Oxygen vacancies (Vo) on the TiO_2 surface lead to the redistribution of two electrons, creating Ti^{3+} sites that are highly reactive due to their unsaturated coordination (Deskins *et al.* 2010). Computational work performed by Pan *et al.* (2009) demonstrated that oxygen defects were more easily created in brookite than in anatase or rutile, and increased the photocatalytic ability in the visible light region. It was shown that oxygen defects on the anatase (101) surface facilitates CO_2 adsorption and charge transfer to the CO_2 molecule (He *et al.* 2010). Since brookite is more readily reduced and oxygen vacancies appear to increase the reactivity of Ti sites, it is of interest to see how oxygen vacancies affect the interaction of the CO_2 molecule with the surface.

Research on iodine doping of TiO_2 was shown to increase the photoactivity of the TiO_2 catalyst (Hong *et al.* 2005; Long *et al.* 2009; Li *et al.* 2011; Zhang *et al.* 2011; Zhang *et al.* 2012; Bagwasi *et al.* 2012; Su *et al.* 2008). Iodine substitution in anatase was more efficient and stable than pristine TiO_2 (Long *et al.* 2009) and the photoactivity of I-doped TiO_2 was on par with P25 in the photooxidation of phenols (Hong *et al.* 2005). The high photoactivity of I-doped TiO_2 was due to strong absorption in the visible and UV light range, band gap narrowing, and the generation of Ti^{3+} surface states (Hong *et al.* 2005). Zhang *et al.* (2011) reported enhanced reduction of CO_2 in the visible and UV light region when using I-doped TiO_2 as compared to undoped TiO_2. It was suggested that the enhanced photoactivity of the I-modified catalyst was the result

15

of a combined effect of the increased surface area, improved charge separation, and the shift in light absorption to the visible range (Zhang *et al.* 2011). However, these studies also resulted in relatively low product production rates. Because it was shown that iodine doping improved the photoactivity of TiO_2 and improved the photoreduction of CO_2 under visible light irradiation, it is worthwhile to see how CO_2 interactions on I-doped anatase (101) and I-doped brookite (210) surfaces compare in terms of the charge transfer to CO_2 and the adsorption energetics.

Computational work was performed to model the interactions of CO_2 on the neutral and negatively-charged brookite TiO_2 (210) surfaces as well as CO_2 interactions on oxygen-deficient brookite (210) surfaces. The results were compared with previously published findings for the interaction of CO_2 on the anatase TiO_2 (101) surface (He *et al.* 2010). Additional computational work was performed to model the interaction of CO_2 on the neutral and negatively-charged anatase (101) and brookite (210) surfaces with iodine doping. The anatase and brookite cluster systems were compared to determine which of the two iodine modified TiO_2 phases interacts more favorably with CO_2. To our knowledge, this is the first computational study of the interaction of CO_2 with the TiO_2 brookite phase and the first computational study of the CO_2 interaction on I-doped anatase and I-doped brookite phases. The information obtained through this work may provide new avenues for further exploration of brookite and mixed-phase brookite TiO_2 as well as further exploration of I-modified TiO_2 as potential photocatalysts for CO_2 reduction.

Chapter 2

CO$_2$ INTERACTION ON UNMODIFIED AND OXYGEN-DEFICIENT

BROOKITE

Introduction: Computational Modeling

Computational modeling has become a widely used tool in many research

areas. Not only can it be a less expensive alternative, it can serve as a supplement

or precursor to experimental work.

Computational tools are useful in providing guidance for material

preparation as well as for predicting bulk properties and mechanisms of

interaction or reaction of species with surfaces (Indrakanti *et al.* 2009; Cramer *et*

al. 2009; Pacchioni 2008; Vittadini *et al.* 2007). Although numerous

computational packages are available to examine solids and surfaces, much of the

recently published computational work has employed programs such as Gaussian

(using Gaussian basis sets) for modeling isolated molecules and the Vienna *Ab*

Initio Simulation Package (VASP), which employs plane waves with

pseudopotentials to model larger surface systems (Cramer *et al.* 2009). The choice

of computational software is usually decided based on whether the calculations

are being performed for isolated molecules or more extended surfaces. Many of

these calculations are based on the use of Density Functional Theory (DFT)

employing different exchange correlation functionals. Example functionals used

for TiO$_2$ systems are the Local Spin Density Approximation (LSDA), gradient

corrected functionals such as Perdew-Burke-Ernzerhof (PBE) or Becke-Lee-

Yang-Parr (BLYP) that are classified as "general gradient approximations" or GGAs, GGAs with a correction for self-interaction (known as GGA+U functionals, where the GGA is typically PBE for TiO_2), or the hybrid functional B3LYP (Cramer *et al.* 2009; Pacchioni 2008; Vittadini *et al.* 2007; Finazzi *et al.* 2008; Labat *et al.* 2007; Lazzeri *et al.* 2001; Diebold *et al.* 2003).

Computational studies that have explored the adsorption of various small molecules onto TiO_2 surfaces have employed a combination of semiempirical techniques as well as DFT techniques (Vittadini *et al.* 2007; Diebold *et al.* 2003; Aschauer *et al.* 2010; Belelli *et al.* 2007; Bruska *et al.* 2009; Homann *et al.* 2004; Scaranto *et al.* 2009). However, DFT calculations provide fundamental "first principles" based information on surface properties that allows for a closer examination of the mechanisms of interaction. Studies examining the interactions of H_2O, CO, CO_2, CH_3OH, and NH_3 on anatase or rutile TiO_2 are just a few examples of the available data.

Understanding how CO_2 interacts with the modified TiO_2 surfaces is important because it may give insights on how electrons are transferred to CO_2 to form energy-bearing compounds. By examining the bond angles associated with adsorption of CO_2 to TiO_2 surfaces, past researchers were able to predict the type of charge transfer that occurred between the surface and the CO_2 (Indrakanti *et al.* 2008; Indrakanti *et al.* 2009). This work was carried out using Gaussian, a program which provides very good representations for isolated molecular systems (Cramer *et al.* 2009). A decreased O–C–O bond angle due to surface interactions was suggested to be indicative of facilitated charge transfer from the surface to

CO_2. Additionally, using computations to investigate the nature of adsorption of molecules on modified TiO_2 materials is critical to understanding and hence predicting the selectivity of the proposed materials. Closely coupling computational and experimental data analysis is critical for developing mechanisms and hence guiding material synthesis to enhance the selectivity of the CO_2 photoreduction reactions.

Computational Method

The interactions of gas-phase CO_2 on the neutral and negatively-charged brookite (210) surfaces were modeled and compared with findings reported for the interaction of CO_2 on the anatase TiO_2 (101) surface (He *et al.* 2010). The brookite TiO_2 surfaces were simulated using cluster models.

In the cluster model, a $Ti_7O_{28}H_{28}$ cluster that was cleaved from the brookite TiO_2 (210) surface was adopted to represent the brookite (210) surface. Six configurations were developed that varied according to the location of the CO_2 molecule over the brookite (210) surface. Stoichiometric TiO_2 in its ground-state is a singlet; therefore, the cluster was cleaved to model a zero-charge singlet cluster in its ground state. The dangling bonds on the oxygen atoms were terminated with hydrogen atoms with an initial bond length of 0.96 Å. The negatively-charged brookite (210) surface was developed by introducing an extra electron into the system, thereby modeling the photoexcited electron. The oxygen-deficient brookite (210) cluster ($Ti_7O_{27}H_{28}$) was generated by removing a bridging oxygen atom in the neutral brookite cluster. Four different

19

configurations were created for the oxygen-deficient brookite cluster, similar to the work reported by He *et al.* (2010) for the anatase system.

All calculations of the cluster models were performed using DFT with the B3LYP functional (Becke 1993; Lee *et al.* 1988). The calculations were implemented using the Gaussian03 program package (Frisch *et al.* 2004). Optimizations of the individual species (CO_2, neutral and negatively-charged $Ti_7O_{28}H_{28}$, and $Ti_7O_{27}H_{28}$) were performed first. The geometries of the various $CO_2 - Ti_7O_{28}H_{28}$ configurations and $CO_2 - Ti_7O_{27}H_{28}$ were then optimized. The adsorption energies of the various $CO_2 - Ti_7O_{28}H_{28}$ and $CO_2 - Ti_7O_{27}H_{28}$ configurations were calculated using the following equation:

$$E_{adsorption} = E_{CO_2-Ti\_cluster} - (E_{CO_2} + E_{Ti\_cluster})$$

All hydroxyl groups were frozen during optimization to mimic the surface environment. The 6-31+G(2df,p) basis set (Ditchfield *et al.* 1971; Hehre *et al.* 1972; Clark *et al.* 1983; Frisch *et al.* 1984) was used for the CO_2 molecule and the five surface oxygen atoms of the brookite cluster. The LanL2DZ basis set (Hay *et al.* 1985; Wadt *et al.* 1985; Hay *et al.* 1985) was used for the remaining oxygen atoms, and all titanium and hydrogen atoms. Vibrational frequencies for all configurations were calculated and scaled by a factor of 0.9652 (Merrick *et al.* 2007). Natural bond orbital (NBO) charge analysis was performed for all cluster calculations.

Results and Discussion

Figure 6 displays the front (Figure 6A) and back side (Figure 6B) of the optimized neutral $Ti_7O_{28}H_{28}$ brookite cluster where atoms 1 and 2 are the 5-coordinated-Ti reaction centers. Ti atom 1 is connected to a 6-coordinated-Ti atom by a 3-coordinated-O atom whereas Ti atom 2 is not connected to a 6-coordinated-Ti atom via an oxygen atom. Instead, the 6-coordinated-Ti atom dangles to the side.

6A   6B
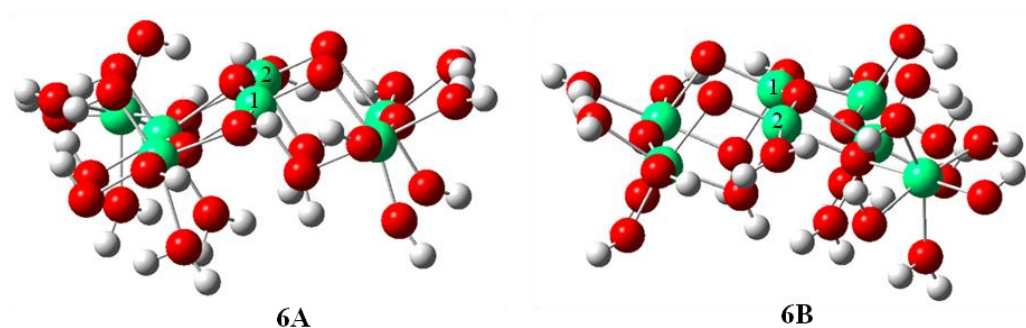
Figure 6: Optimized geometry of the neutral $Ti_7O_{28}H_{28}$ cluster representing the brookite (210) surface; 6A represents the front side of the cluster and 6B shows the back side of the cluster. Symbols for the individual atoms are: Ti in green, O in red, and H in white.

CO_2 Adsorbed to the Brookite (210) Surface

Figure 7 displays the various configurations of CO_2 interacting with the neutral brookite (210) surface. A total of five distinct configurations exist, and are labeled 7A-7E. For better viewing, two images of configuration 7E are provided and are labeled 7E(a) and 7E(b). Figure 8 displays the various

configurations of CO_2 adsorbed to the negatively-charged brookite (210) surface. A total of five distinct configurations were found. They are labeled 8A-8E. Two images of configuration 8E are provided and are labeled 8E(a) and 8E(b).

Additional work was undertaken to determine whether a brookite surface that contained oxygen vacancies would more favorably adsorb CO_2 and facilitate charge transfer to the CO_2 molecule. The bridging oxygen atom of the first 5-coordinated-Ti atom was removed from the cluster system. Figure 9 displays the optimized configurations of CO_2 adsorbed to the oxygen-deficient brookite surface cluster. The ground states of configurations 9A, 9B, and 9 D are singlet states and the ground state of the 9C configuration is a triplet state.
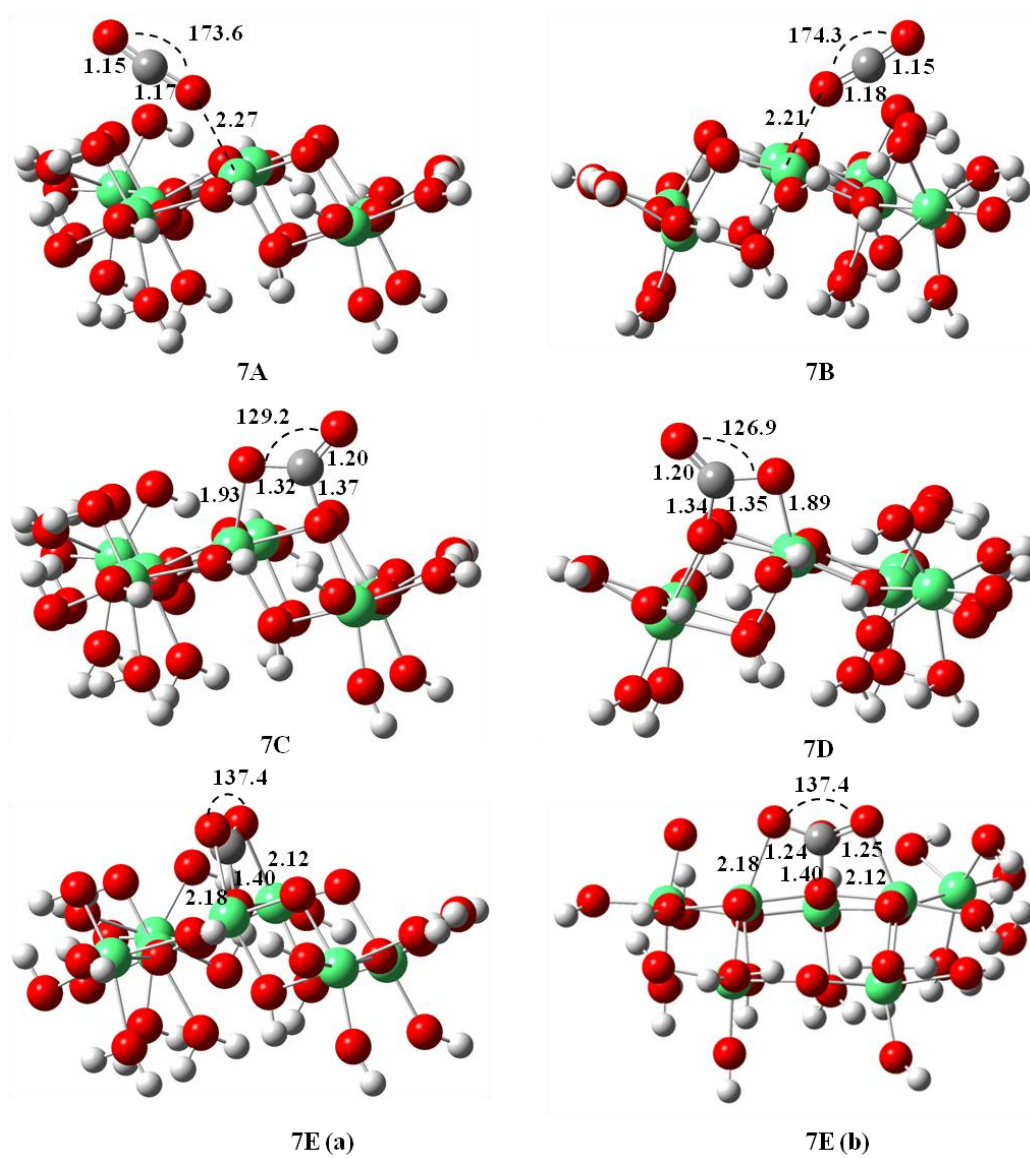
Figure 7: Optimized geometry configurations of CO_2 adsorbed onto the neutral $Ti_7O_{28}H_{28}$ cluster. Colors represent atoms accordingly: Ti in green, O in red, H in white, and C in gray. Distances and angles are in Å and degrees, respectively.
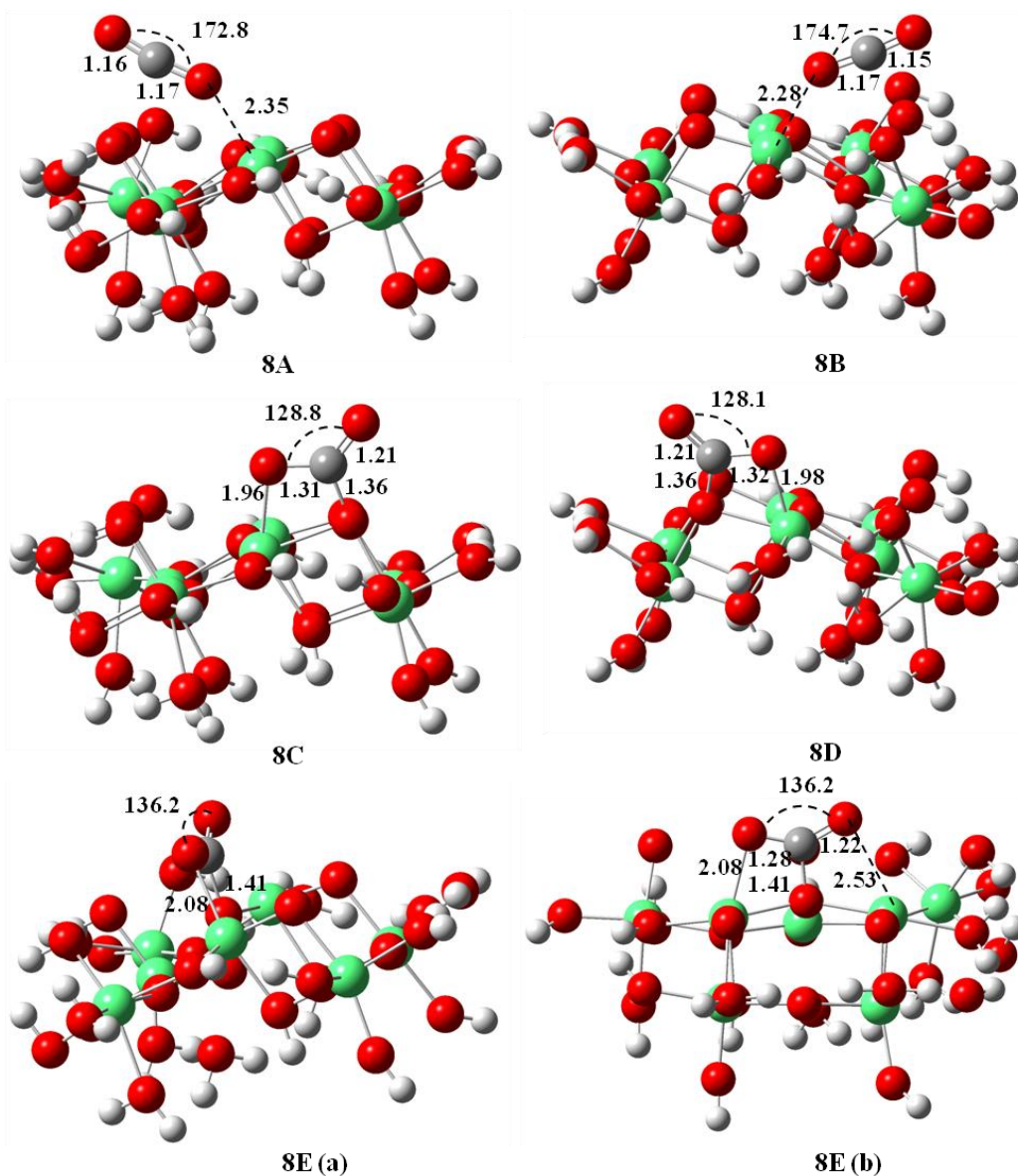
Figure 8: Optimized geometry configurations of CO_2 adsorbed onto the negatively-charged $Ti_7O_{28}H_{28}$ cluster. Colors represent atoms accordingly: Ti in green, O in red, H in white, and C in gray. Distances and angles are in Å and degrees, respectively.
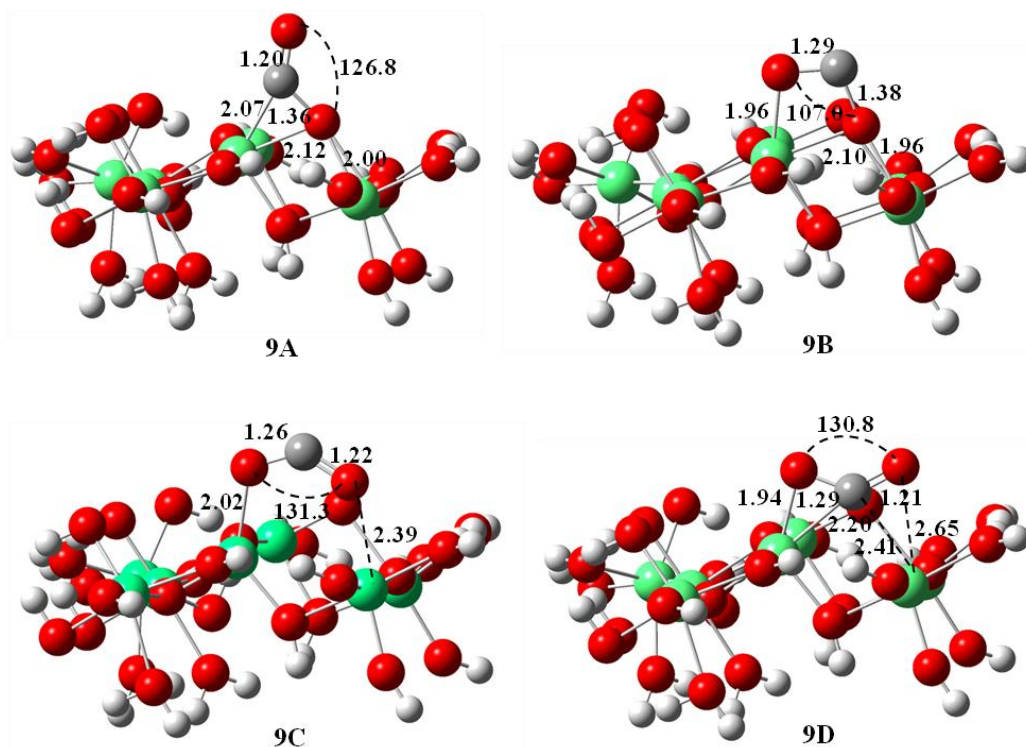
Figure 9: Optimized geometry configurations of CO_2 adsorbed on the cluster system of brookite (210) surface with an oxygen vacancy. Colors represent atoms accordingly: Ti in green, O in red, H in white, and C in gray. Distances and angles are in Å and degrees, respectively.

Table 2 reports the calculated adsorption energies (in eV) of CO_2 bound to the neutral and negatively-charged brookite surfaces as well as the neutral and negatively-charged anatase surfaces. Adsorption energies of CO_2 adsorbed onto the oxygen-deficient brookite and anatase surfaces are also provided in Table 2 for the cluster system.

Table 2: Calculated Adsorption Energies (in eV) of CO$_2$ on the Neutral, Negatively-Charged, and Oxygen-Deficient Brookite (210) and Anatase (101) Surfaces.

Phase	Brookite (210)			Anatase (101)[a]		
State	Neutral (Configuration 7)	Negatively-Charged (Configuration 8)	Oxygen-Deficient (Configuration 9)	Neutral	Negatively-Charged	Oxygen-Deficient
A	-0.44	-0.36	-1.53	-0.34	-0.35	-1.09
B	-0.50	-0.41	-0.92	_[b]	_[b]	-0.36
C	-0.30	-0.51	-0.51	-0.41	-0.35	0.08
D	-0.72	-0.90	-1.59	_[b]	_[b]	-0.97
E	0.33	0.08	_[b]	0.22	0.21	_[b]
F	_[b]	_[b]	_[b]	_[b]	0.33	_[b]

[a] Adsorption energies (in eV) of CO$_2$ adsorbed onto neutral, negatively-charged, and oxygen-deficient anatase (101) surfaces reported by He *et al.* (2010).

[b] The dashed lines indicate structures converged to already optimized configurations.

As can be seen from Figures 7 and 8, CO_2 interacts with both the neutral and negatively-charged brookite (210) surface in similar binding configurations. The binding site for configurations A and C is located on a 5-coordinated-Ti atom 1. In configurations B and D, the binding site is located on the second 5-coordinated-Ti atom with the dangling 6-coordinated-Ti atom. Configuration E for both the neutral and negatively-charged brookite surfaces have significant differences. In configuration 7E, both oxygen atoms of the CO_2 bind to the 5-coordinated-Ti atoms to form a polydentate carbonate. On the negatively-charged brookite surface only one oxygen atom binds to a 5-coordinated-Ti atom. The binding site occurs on the 5-coordinated-Ti atom connected to the 6-coordinated-Ti atom.

On the neutral brookite cluster, in configurations 7B and 7D, CO_2 binds more closely to the surface and experiences a stronger adsorption (Table 2) than configurations 7A and 7C. It is worth noting that on the brookite (210) surface, although 7B is lower in energy (-0.50 eV) than configuration 7A (-0.44 eV), the energetic difference (-0.06 eV) is within the errors of the calculation, thus making the two configurations energetically equivalent. Of the five configurations, configuration 7D has the lowest adsorption energy (-0.72 eV), making it the most likely binding formation to occur on the neutral brookite (210) surface. Configuration 7E, which forms a polydentate carbonate, has the highest adsorption energy (0.33 eV) and is therefore the least likely to exist.

On the negatively-charged brookite cluster, configurations 8C and 8D are the more energetically favorable binding forms with adsorption energies of -0.51

27

eV and -0.90 eV, respectively. Although the CO_2 in configuration 8B binds closer to the negatively-charged brookite surface and has a lower CO_2-surface adsorption energy than configuration 8A, both configurations remain energetically competitive. Configuration 8E is the most energetically unfavorable with an adsorption energy of 0.08 eV.

In comparing the neutral and negatively-charged cluster systems, the negatively-charged brookite surfaces appear to be more reactive. Configurations 8C, 8D, and 8E have significantly lower adsorption energies than their neutral counterparts with the exception of 7B, which has an adsorption energy similar to configuration 8C.

CO_2 more readily adsorbs to the brookite surface that has the oxygen vacancies. As can be seen from Table 2, configurations 9A, 9B, 9C, and 9D have more favorable CO_2 adsorption energies than both the neutral and negatively-charged brookite (210) surfaces. Configurations 9A and 9D have comparable adsorption energies, which are significantly lower than 8B and much more favorable that the most stable configuration on both the neutral and negatively-charged brookite surfaces. Configuration 9B is energetically equivalent to the most stable configuration (8D) on the negatively-charged brookite surface and more favorable than the most stable configuration (7D) on the neutral brookite surface. Configuration 9C, although it is the least energetically favorable of the four configurations, its adsorption energy is still comparable to configurations 7A, 7B, and 8C.

Comparison of CO_2 Adsorption to the Brookite (210) and the Anatase (101)

Surfaces

Configurations 7A, 7C, and 7E are structurally similar to the binding

configurations calculated by He *et al.* (2010) for the neutral anatase (101) surface.

Two additional configurations exist on the surface of the brookite (210) cluster,

configurations 7B and 7D.

The negatively-charged brookite surface configurations 8A and 8C are

structurally similar to the binding configurations calculated by He *et al.* (2010) for

the negatively-charged anatase (101) surface. Three new configurations exist on

the brookite (210) surface, configurations 8B, 8D, and 8E. As was described

previously, only one oxygen atom from the CO_2 molecule of configuration 8E

binds to the negatively-charged brookite surface. On the negatively-charged

anatase surface, both oxygen atoms from the CO_2 molecule bind to the two 5-

coordinated-Ti atom sites, forming a polydentate carbonate. No configuration

similar to F exists for the brookite surface. Configuration F on the negative

anatase surface had a CO_2 as a bridging bidentate with the carbon atom pointing

upwards and the oxygen atoms bound to the two 5-coordinated-Ti atoms (He *et*

al. 2010).

In Table 2, the adsorption energies for the binding configurations of both

the neutral and negatively-charged brookite (210) surfaces and the anatase (101)

surfaces are presented and labeled A-E. As seen with previous DFT calculations

(Li *et al.* 2008), the brookite (210) surface affects the adsorptive ability of

molecules and in some cases, creates stronger binding sites.

In the case of the neutral brookite and anatase surfaces cluster systems, configuration A has a significantly lower adsorption energy in the brookite (210) surface than in the anatase (101) surface. Additionally, the brookite surface allows for the formation of two additional binding configurations (B and D) that have much lower (more favorable) adsorption energies than any of the configurations formed on the anatase surface. This implies that the neutral brookite (210) surface allows for stronger binding sites than the neutral anatase (101) surface.

On the negatively-charged brookite and anatase surfaces, configuration A is structurally and energetically similar. Although configuration C for both surfaces is structurally similar, that of brookite has a lower adsorption energy and is therefore more favorable. Configurations B and D are two additional configurations formed on the negatively-charged brookite surface that exhibit much lower adsorption energies than configurations on the negatively-charged anatase surface. Configurations A and B for both brookite and anatase and configuration C for anatase are energetically equivalent. Configuration D is the most favorable of the structures with an adsorption energy of -0.90 eV while configurations E and F are the most unstable with configuration F non-existent on the brookite surface.

In the oxygen-deficient brookite system, configurations 9A, 9B, 9C, and 9D have geometries similar to those on the oxygen-deficient anatase (101) surface with distances and bond angles differing by 0.01 to 0.16 Å and 0.1 to 1.9°, respectively. The adsorption energies are significantly more favorable on the

30

brookite surface than on the anatase surface. The respective adsorption energies

of 9A, 9B, 9C and 9D are -1.53 eV, -0.92 eV, -0.51 eV, and -1.59 eV whereas the

corresponding adsorption energies on the anatase surface are -1.09 eV, -0.36 eV,

0.08 eV and -0.97 eV (He *et al.* 2010). This suggests that CO_2 is more likely to

experience stronger interactions with the oxygen-deficient brookite (210) surface

than with the oxygen-deficient anatase (101) surface. Most notable is the

significantly lower adsorption energy of the 9C configuration which is 0.59 eV

lower than the corresponding anatase configuration.

Charge and Spin Density Analyses of CO_2 Adsorbed on the Brookite (210)

Surface

Several reported studies have demonstrated the ability of the anatase TiO_2

to reduce CO_2 to fuels (Linsebigler *et al.* 1995; Koci *et al.* 2008; Kitano *et al.*

2007; Li *et al.* 2010; Tseng *et al.* 2004; Koci *et al.* 2010; Anpo *et al.* 2010;

Varghese *et al.* 2009; Yang *et al.* 2009; Indrakanti *et al.* 2009; He *et al.* 2010).

The formation of the CO_2^- on the surface of TiO_2 is considered the first step in the

reduction of CO_2 (Centi *et al.* 2009). The reduction of CO_2 to this anionic state is

accompanied by a signature bending from its linear form (Figure 10A) to an O-C-

O angle of ~ 138°. This deformation is shown in Figure 10B. Adsorbed CO_2^-

also has two signature bands at 1640 and 1219 cm^{-1} (Rasko *et al.* 1994).
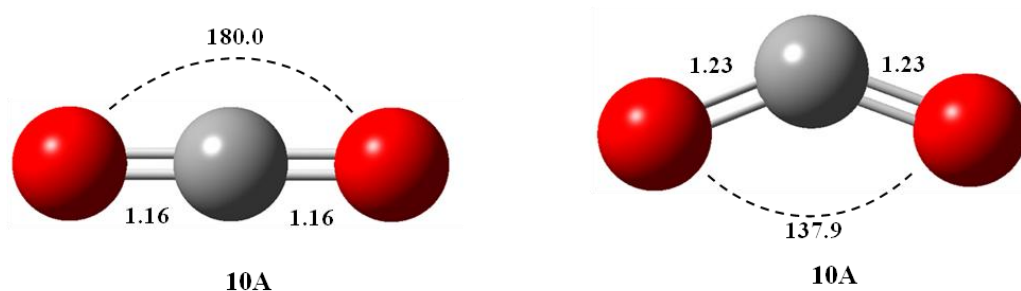
Figure 10: Optimized geometries of CO_2 and CO_2^- using B3LYP/6-31+G(2df, p) level. Colors represent atoms accordingly: O in red and C in gray. Distances and angles are in Å and degrees, respectively.

He *et al.* (He *et al.* 2010) demonstrated the ability of the anatase (101) surface to reduce CO_2 to its anionic form. Although highly unstable, as is shown by the high adsorption energies for configuration F and only stabilized on the negatively-charged anatase (101) surface, charge analysis demonstrated a net charge transfer to the CO_2 and most notably to the carbon (Table 3). The calculated vibrational frequency values (1638 and 1265 cm^{-1}) (He *et al.* 2010) corresponded well with the band values for the CO_2^-. However, no such configuration exists on the brookite surface through our calculations. Charge, spin density, and vibrational frequency calculations on the CO_2 –brookite configurations confirm that there is no CO_2^- formation on the brookite (210) surface.

In Table 3, the charge and spin densities of CO_2 of the different configurations on the neutral and negatively-charged brookite and anatase surfaces are reported. Table 3 also provides the CO_2 charge values for the

oxygen-deficient brookite and anatase cluster surfaces. The charge values are the sum of the NBO atomic charges on CO_2.

In comparing the neutral and negatively-charged brookite surface cluster system, one can see from Table 3 that configurations 7C - 7E (neutral) and 8C - 8E (negatively-charged) have a negative charge on the CO_2 molecule. The spin density was calculated to determine if an unpaired electron exists on the CO_2 molecule. From Table 3, it can be seen that the spin density located on the CO_2 is minute for all configurations. In other words, the unpaired electron on the surface is not transferred to the CO_2 molecule. Figure 11 depicts the spin densities of the various binding configurations for the negatively-charged brookite surface cluster. On all configurations, it can be seen that charge transfer occurs in the direction of the second 5-coordinated-Ti atom, demonstrating that the unpaired electron is located primarily on the second 5-coordinated-Ti atom and not on the CO_2 molecule. This suggests that the 5-coordinated-Ti atom prefers to hold onto the unpaired electron instead of sharing it with the CO_2.

Table 3: Charge and Spin Distributions of CO_2 on the Neutral, Negatively-Charged, and Oxygen-Deficient Brookite (210) and Anatase (101) TiO_2 Surfaces.

Phase	Brookite (210)					Anatase (101)[a]				
State	Neutral (Configuration 7)	Negatively-Charged (Configuration 8)		Oxygen-Deficient (Configuration 9)		Neutral	Negatively-Charged		Oxygen-Deficient	
	Charge	Charge	Spin	Charge		Charge	Charge	Spin	Charge	
A	0.17	0.14	0.00	-0.50		0.10	0.09	0.03	-0.63	
B	0.18	0.14	0.01	-0.77		--[b]	--[b]	--[b]	-0.91	
C	-0.16	-0.23	0.00	-0.41		-0.23	-0.31	0.01	-0.50	
D	-0.16	-0.30	-0.01	-0.41		--[b]	--[b]	--[b]	-0.57	
E	-0.03	-0.11	0.01	--[b]		-0.18	-0.16	0.00	--[b]	
F	--[b]	--[b]	--[b]	--[b]		--[b]	-0.45	0.87	--	

[a] Charge and spin distribution of CO_2 adsorbed onto neutral, negatively charged, and oxygen-deficient anatase (101)

surfaces reported by He *et al.* (2010).

[b] The dashed lines indicate structures converged to already optimized configurations.

34
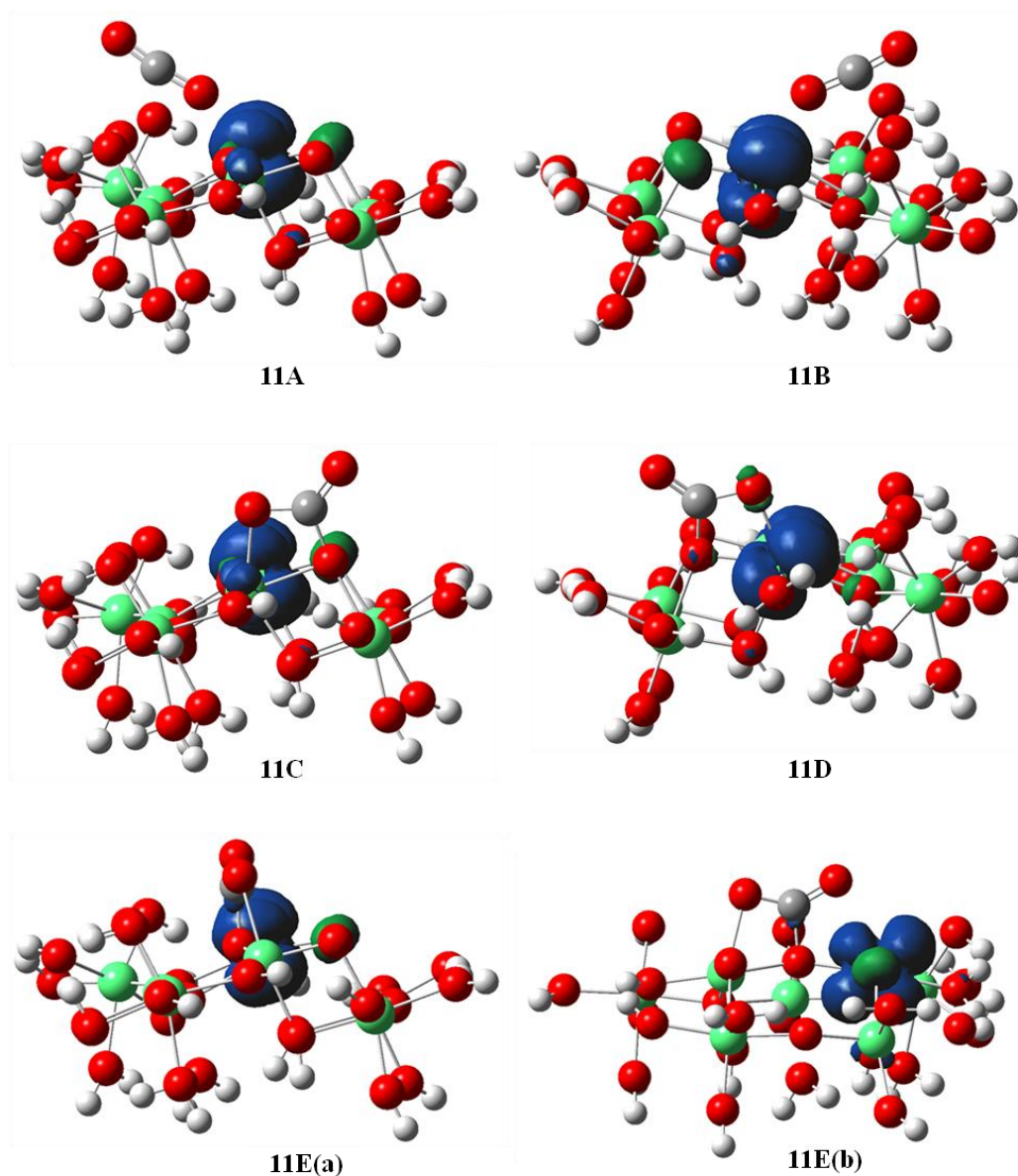
Figure 11: Spin densities of CO_2 binding configurations on the negatively-charged brookite (210) TiO_2 surface. Colors represent atoms accordingly: Ti in green, O in red, H in white, and C in gray. Blue represents unpaired electron.

The charge on the CO_2 molecule on oxygen-deficient brookite is larger than on either the neutral or negatively-charged brookite surfaces, confirming that oxygen-deficient brookite facilitates charge transfer to the CO_2 molecule. On the

oxygen-deficient anatase surface, the charge transfer is only slightly larger than that of the brookite surface. Similar to the anatase cluster system, the 9C configuration is in a triplet state with a spin located on the CO_2 molecule, most notably on the carbon atom and a spin on a 5-coordinated-Ti atom (see Figure 12). This confirms that oxygen vacancies aid in the formation of CO_2^- with a greater likelihood of its formation on the brookite surface than on the anatase surface.
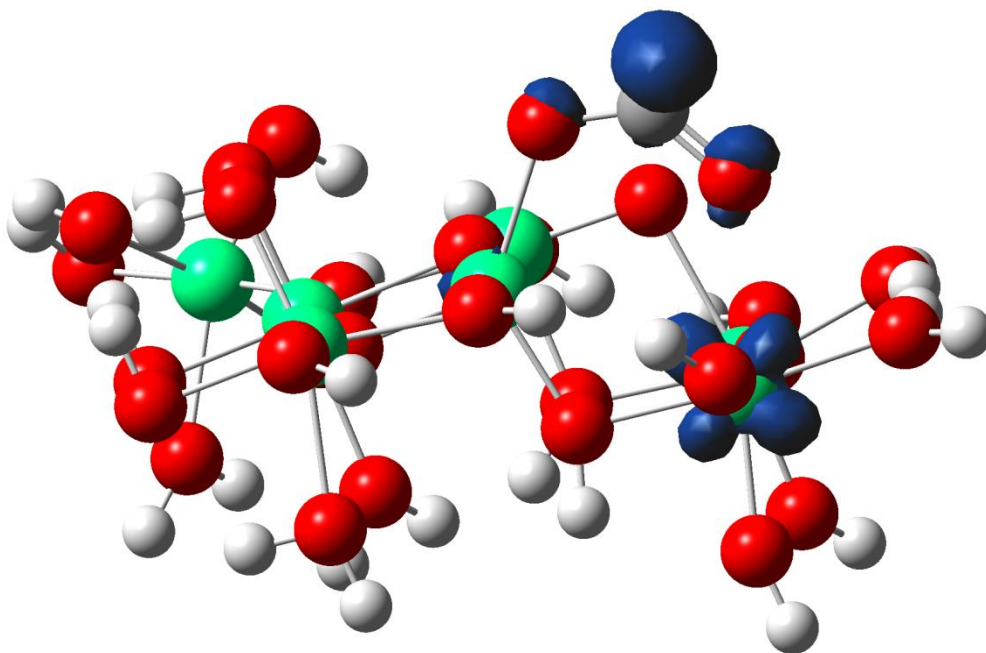
Figure 12: Spin density of configuration 9C. 9C has a triplet state. Colors represent atoms accordingly: Ti in green, O in red, H in white, and C in gray. Blue represents unpaired electron.

Collaborative work with Dr. Xihong Peng at Arizona State University, Polytechnic Campus, was performed on perfect brookite (210) periodic slab

systems using VASP. The computational work produced similar CO_2

configurations to the brookite cluster system charge and spin density trends.

Vibrational Frequency Analysis of CO_2 Adsorbed on the Brookite (210) Surface

The vibrational frequencies were quantified computationally for each

configuration to help identify the adsorbed CO_2 species, including the CO_2^-.

Table 4 presents the computationally calculated vibrational frequencies in cm^{-1}.

Table 4: Calculated Vibrational Frequencies (in cm^{-1}) of Bending (v_2), Symmetric

Stretching (v_1), and Asymmetric Stretching (v_3) Modes of CO_2 on the Neutral,

Negatively-Charged, and Oxygen-Deficient Brookite (210) Surfaces [a]

		Brookite (210) Surface				
	Mode	A	B	C	D	E
	v_2	623, 639	649	772	779	778
Neutral	v_1	1332	1326	987	985	1253
	v_3	2347	2347	1764	1770	1710
	v_2	638	644	780	788	776
Negatively-charged	v_1	1328	1327	1004	1005	1223
	v_3	2337	2345	1729	1715	1738
	v_2	738	761, 742	716, 725	744, 761	--
Oxygen-deficient	$v_1^{[b]}$	891	866	1275	1142	--
	$v_3^{[b]}$	1758	1248	1659	1702	--

[a]Vibrational frequencies were scaled by a factor of 0.9652 (Merrick et al 2007).

[b]Vibrational modes v_1 and v_3 assigned to configurations A and B are for two C-O

stretching modes other than symmetric and asymmetric stretching modes.

We first examined the neutral and negatively-charged systems. For

configurations A and B, the calculated vibrational frequencies (Table 4)

correspond well with the reported band values of adsorbed linear CO_2 (Henderson 1998; Ramis *et al.* 1991). The values are also in good agreement with the computational findings of adsorbed linear CO_2 reported by He *et al.* (2010). Configurations C – E have vibrational frequencies that are most consistent with side-on bonded CO_2 on cationic sites (Ramis *et al.* 1991). Rasko *et al.* (1994) identified two signature absorptions bands (1640 and 1219 cm^{-1}) attributed to bent CO_2^-. From Table 4, no configurations on the neutral and negatively-charged brookite (210) surface have vibrational frequencies that relate to both of the reported signature bands.

Configurations C, D, and E for the neutral and negatively-charged cluster system have a net charge transfer (Table 2). However, charge analysis suggests that the net charge transfer to the carbon atom of the CO_2 molecule for any of the configurations is negligible. Although configuration E for the neutral and negatively-charged surfaces both exhibit the characteristic bending that is accompanied with the formation of the CO_2^-, the CO_2 molecule lacks notable charge and spin as well as vibrational frequency values (Table 4) associated with the signature bands of CO_2^- as reported by Rasko *et al.* (1994). Additionally, the frequencies do not compare well with the values reported in previous experimental studies (Yang *et al.* 2010; Su *et al.* 2008). Configurations C and D also lack vibrational frequency values characteristic of the CO_2^-. As suggested by Indrakanti *et al.* (2008), configuration E can be thought of as an exception in that CO_2 experiences charge transfer, although miniscule, and undergoes bending but the carbon atom is not reduced. The lack of the characteristic bands and

38

insignificant charge transfer to the CO_2 molecule for any of the configurations on the neutral and negatively charged brookite (210) surface suggest that there was no CO_2^- formation.

Table 4 also presents the vibrational frequency data for CO_2 adsorbed onto the brookite (210) surface with oxygen vacancies. Shifts in vibrational frequencies were expected when considering the geometry and bonding of the structures. Noticeable shifts occur primarily for v_1 vibrational modes.

Configuration 9C is the most interesting structure of the four because of its resemblance to the CO_2^-. Additionally, the calculated vibrational frequency bands (1275 cm^{-1} and 1659 cm^{-1}) are similar to reported bands for CO_2^- (Rasko *et al.* 1994; Yang *et al.* 2010; Su *et al.* 2008). These bands also agree well with additional collaborative experimental work on the interaction of CO_2 with brookite and oxygen-deficient brookite performed by Professor Ying Li and his research group at the University of Wisconsin-Milwaukee. Using Fourier Transform Infrared (FTIR) spectroscopy equipped with a Diffuse Reflectance Infrared Fourier Transform Spectroscopy (DRIFTS) system, they identified adsorption bands (1248 cm^{-1} and 1672 cm^{-1}) of the CO_2 anion on oxygen-deficient brookite and not on perfect brookite. The O-C-O angle (131.3°) of configuration 9C is not the characteristic ~ 138° associated with the CO_2^-, but it is close. The increased charge transfer, similar vibrational frequency bands, and O-C-O angle near 138° suggest that configuration 9C may be a precursor to the CO_2^- formation.

It is suggested that the CO_2 molecule becomes easier to reduce as the O-C-O bond angle decreases from 180° (Indrakanti *et al.* 2008). With increased

charge transfer to the CO_2 molecule and the decreased O-C-O angle, it is likely that configurations 9A, 9B, 9C and 9D are precursors to CO_2 reduction. The more favorable adsorption energies and increased charge transfer suggest that oxygen vacancies on the brookite (210) surface favor bent CO_2 configurations and aid in the stabilization of negatively-charged CO_2^-.

Chapter 3

CO2 INTERACTION ON IODINE-DOPED ANATASE AND BROOKITE

Introduction

One of the major goals of photocatalytically reducing CO_2 is to utilize

visible light to activate the catalyst and initiate CO_2 photoreduction. Iodine

doping of TiO_2 has demonstrated its ability to increase the photoactivity of TiO_2

under visible light (Hong *et al.* 2005; Long *et al.* 2009). Regarding CO_2

photoreduction, Zhang *et al.* (2011) and Zhang *et al.* (2012) reported an enhanced

reduction of CO_2 under visible light compared to undoped TiO_2. By analyzing the

charge transfer to CO_2 in both I-doped anatase (101) and I-doped brookite (210)

surfaces and the adsorption energetics of each CO_2–I-doped TiO_2 system,

potential and new photocatalysts in the form of I-modified TiO_2 can be further

investigated and developed.

Computational Methods

The interactions of gas phase CO_2 on the neutral and negatively-charged

iodine-doped anatase (101) and iodine-doped brookite (210) surfaces were

modeled and compared. The iodine-doped TiO_2 surfaces were simulated using

cluster model systems.

The anatase (101) surface was modeled by a $Ti_{10}O_{37}H_{34}$ cluster which was

cleaved from the anatase (101) TiO_2 surface. A $Ti_{10}O_{38}H_{36}$ cluster was adopted to

represent the brookite (210) surface and was cleaved from the brookite TiO_2 (210) surface. Stoichiometric TiO_2 in its ground-state is a singlet; therefore, the cluster was cleaved to model a zero-charge singlet cluster in its ground state. The dangling bonds on the oxygen atoms were terminated with hydrogen atoms with an initial bond length of 0.96 Å. The iodine-doped anatase (101) and brookite (210) clusters (I-anatase, I-$Ti_9O_{37}H_{34}$, I-brookite, I-$Ti_9O_{38}H_{36}$) were generated by replacing the center 5-coordinated Ti atom with an I atom. Because a Ti^{4+} is being replaced by a I^{5+}, an unpaired electron was produced in the system. This resulted in an I-TiO_2 zero-charge doublet cluster. The negatively-charged I-doped anatase (101) and I-doped brookite (210) surfaces were developed by introducing an extra electron into the system, thereby modeling the photoexcited electron. Configurations were developed for each iodine-doped cluster that varied according to the location of the CO_2 molecule over the anatase (101) and brookite (210) surfaces. The different configurations created for the iodine-doped anatase and brookite clusters were similar to the configurations reported by He *et al.* (2010).

All calculations were performed using DFT with the B3LYP functional (Becke 1993; Lee *et al.* 1988). The calculations were implemented using the Gaussian03 program package (Frisch *et al.* 2004). Optimizations of the CO_2, $Ti_{10}O_{37}H_{34}$ cluster, and $Ti_{10}O_{38}H_{36}$ clusters were performed first. An iodine atom was doped into the optimized $Ti_{10}O_{37}H_{34}$ and $Ti_{10}O_{38}H_{36}$ clusters to produce the I-doped anatase cluster (I-$Ti_9O_{37}H_{34}$) and the I-doped brookite cluster (I-$Ti_9O_{38}H_{36}$). These clusters were then optimized. The geometries of the various CO_2 – I-

42

$Ti_9O_{37}H_{34}$ configurations and $CO_2 - I\text{-}Ti_9O_{38}H_{36}$ were then optimized. The adsorption energies of the various $CO_2 - I\text{-}Ti_9O_{37}H_{34}$ and $CO_2 - I\text{-}Ti_9O_{38}H_{36}$ configurations were calculated using the following equation:

$$E_{adsorption} = E_{CO_2-I\_Ti\_cluster} - (E_{CO_2} + E_{I\_Ti\_cluster})$$

All hydroxyl groups were frozen during optimization to mimic the surface environment. The 6-31+G(2df,p) basis set (Ditchfield *et al.* 1971; Hehre *et al.* 1972; Clark *et al.* 1983; Frisch *et al.* 1984) was used for the CO_2 molecule and the eight surface oxygen atoms of the anatase and brookite clusters. The LanL2DZ basis set (Hay *et al.* 1985; Wadt *et al.* 1985; Hay *et al.* 1985) was used for the remaining oxygen atoms, the iodine atoms, and all titanium and hydrogen atoms. NBO charge analysis was performed for all cluster calculations.

Results and Discussion

Figure 13 displays the front views of the optimized neutral (Figure 13A) and negatively-charged (Figure 13B) I-doped anatase (101) clusters, and Figure 14 displays the front views of the optimized neutral (Figure 14A) and negatively charged (Figure 14A) I-doped brookite (210) clusters. Titanium atoms #1-Ti and #2-Ti are the 5-coordinated-Ti reaction centers. In both the anatase and brookite clusters, warping occurs in the lattice where the iodine is present. This warping increases in the negatively-charged system with the iodine atom protruding out to a side. Because of the lattice warping due to the iodine, CO_2 was interacted with both adjacent Ti reaction centers.
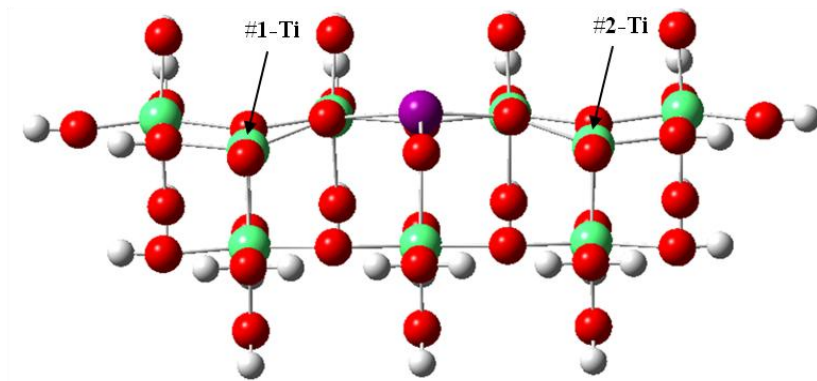
13A
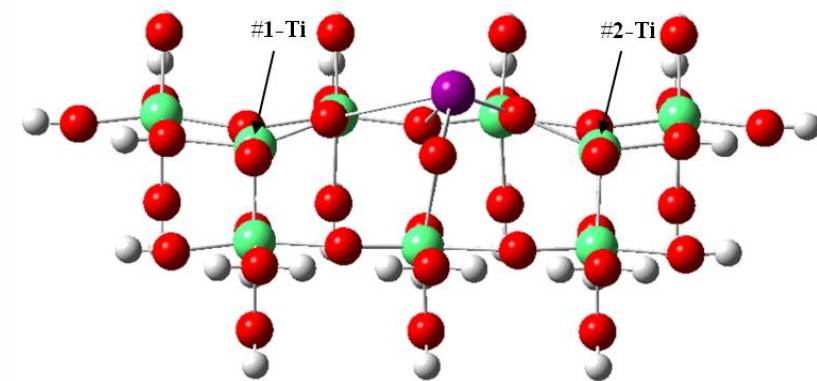
13B

Figure 13: Optimized geometry of the neutral (A) and negatively-charged (B) I-doped TiO_2 cluster representing the anatase (101) surface. Symbols for the individual atoms are: Ti in green, O in red, H in white, and I in purple.

14A
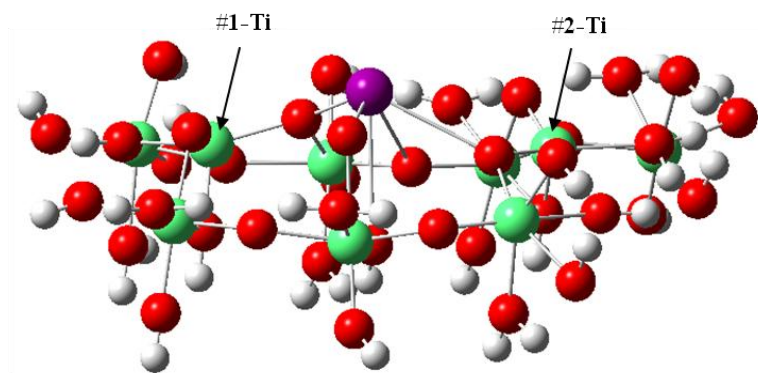
14B

Figure 14: Optimized geometry of the neutral (A) and negatively-charged (B) I-doped TiO_2 cluster representing the brookite (210) surface. Symbols for the individual atoms are: Ti in green, O in red, H in white, and I in purple.

CO$_2$ Adsorbed to the I-Doped Anatase (101) and I-Doped Brookite (210) Surface

Figures 15, 16, 17, and 18 display the various configurations of CO$_2$ interacting with the neutral I-doped anatase (101), negatively-charged I-doped anatase (101), neutral I-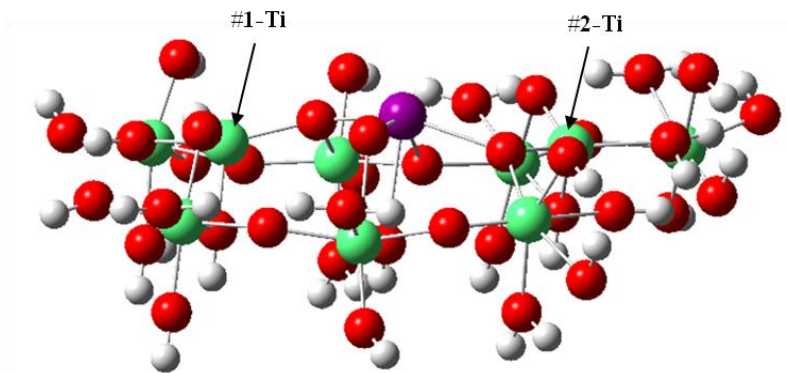doped brookite (210), and negatively-charged I-doped brookite (210) surfaces, respectively. A total of three distinct configurations exist on the neutral I-doped anatase surface, and are labeled 15A-15C. Two images of configuration 15C are provided for better viewing, and are labeled 15C(a) and 15C(b). The negatively-charged I-doped anatase surface has five distinct configurations that are labeled 16A-16C. The negatively-charged I-doped anatase system has more configurations because the presence of the negative charge resulted in warping that significantly affected the overall symmetry whereas in the neutral I-doped anatase system symmetry was maintained which affected the charge distribution. Five distinct configurations are found for both the neutral and negatively-charged I-doped brookite (210) surfaces. The configurations on the neutral I-doped brookite surface are labeled 17A-17E. On the negatively-charged I-doped brookite surface, the configurations are labeled 18A, 18B, and 18D-18F. For all neutral and negatively-charged systems, the CO$_2$ in configurations A-C binds to #1-Ti atom and in configurations D-F it binds to #2-Ti atom. Configurations A, B, D, and E are side views of the TiO$_2$ cluster from their respective Ti reaction center. Configurations 15C(a), 16C, 17C(a) and 18F show front views of the TiO$_2$ cluster from their respective Ti reaction center.
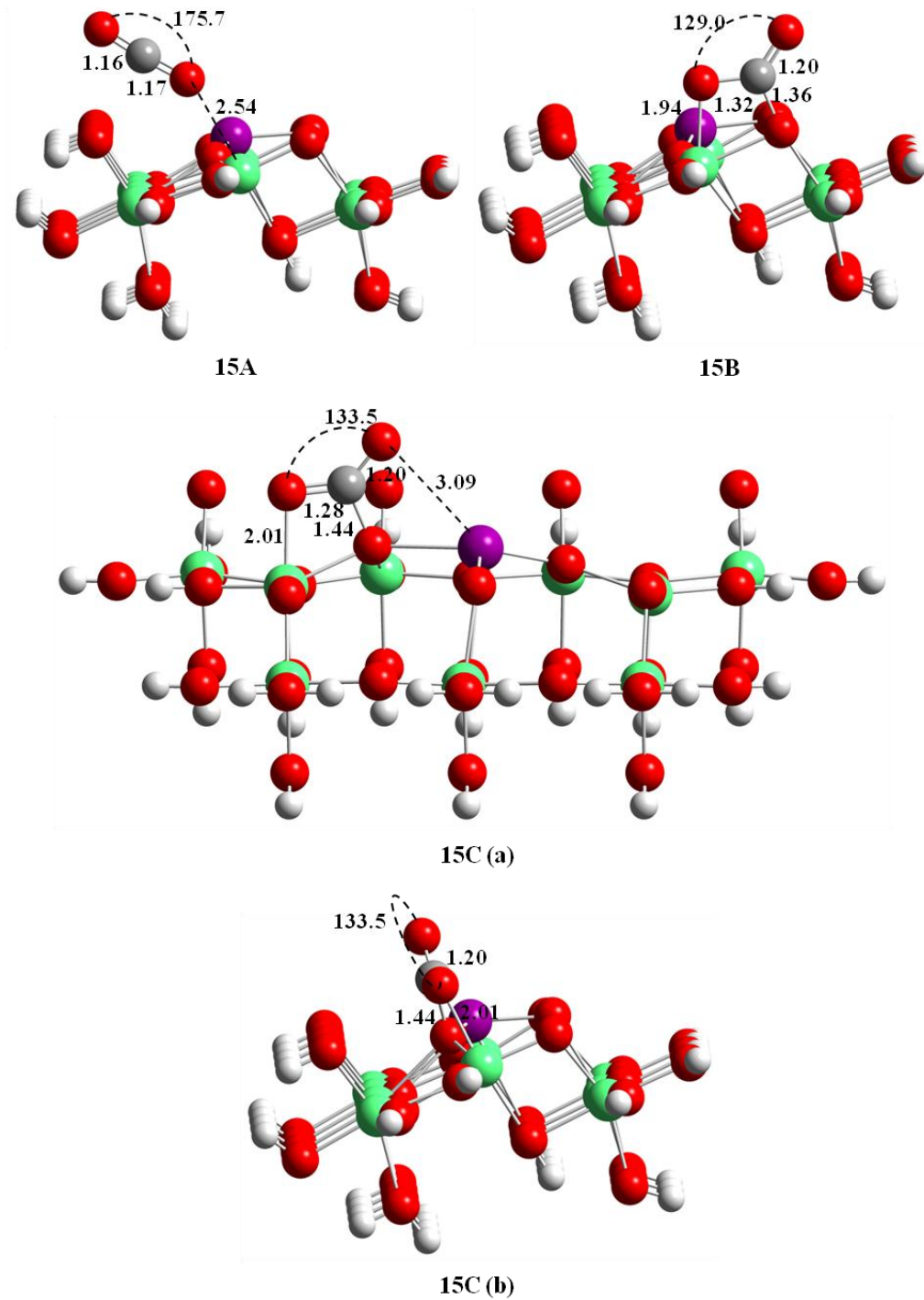
Figure 15: Optimized geometry configurations of CO_2 adsorbed onto the neutral I-doped anatase (101) surface cluster. Colors represent atoms accordingly: Ti in green, O in red, H in white, C in gray, and I in purple. Distances and angles are in

Å and degrees, respectively. Configuration 15C has two images presented for better viewing; a front view, 15C(a), and a side view, 15C(b).

16A

16D

16B

16E

16C
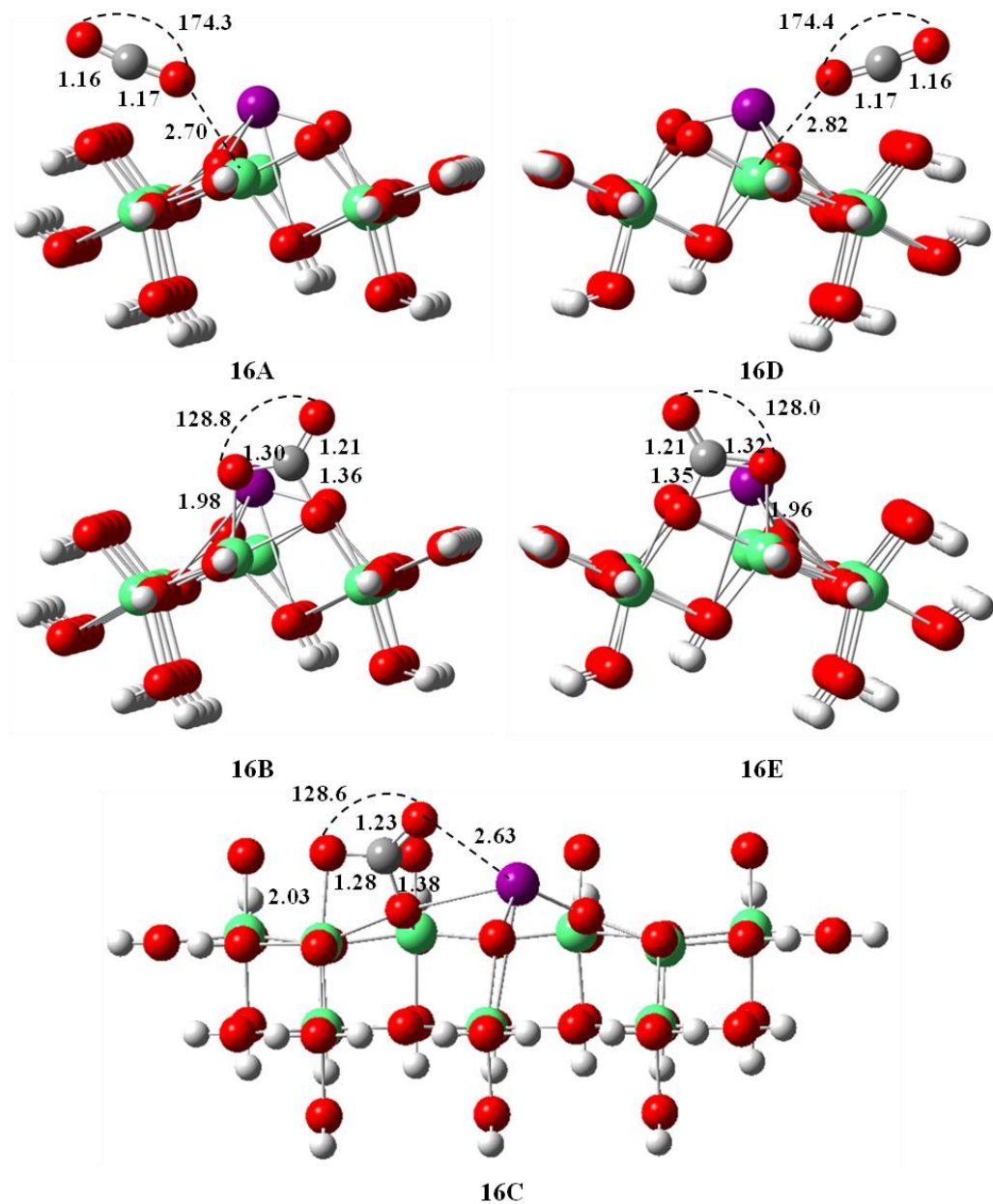
Figure 16: Optimized geometry configurations of CO_2 adsorbed onto the negatively-charged I-doped anatase (101) surface cluster. Colors represent atoms

accordingly: Ti in green, O in red, H in white, C in gray, and I in purple.

Distances and angles are in Å and degrees, respectively.

17A

17D

17B

17E

17C (a)

17C (b)

50
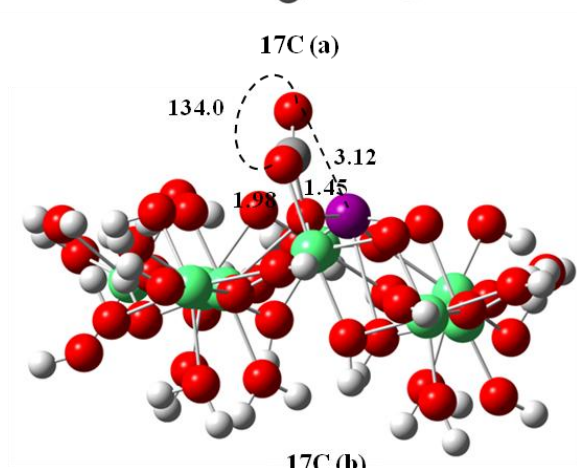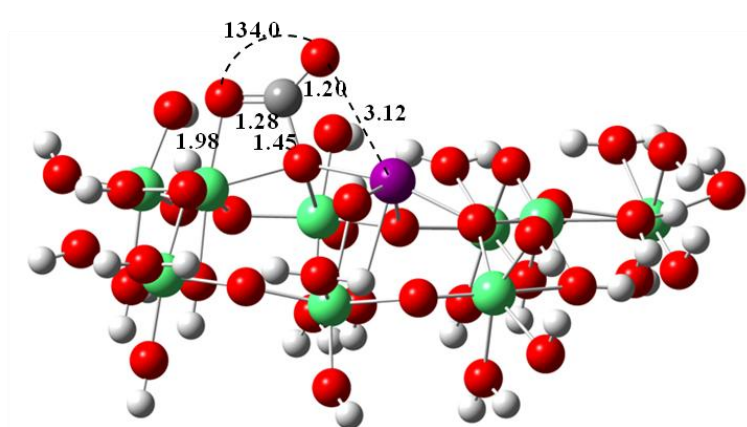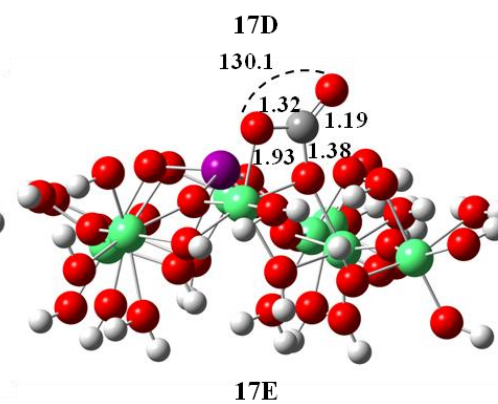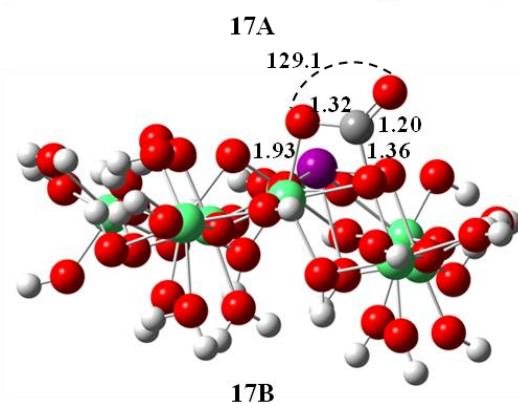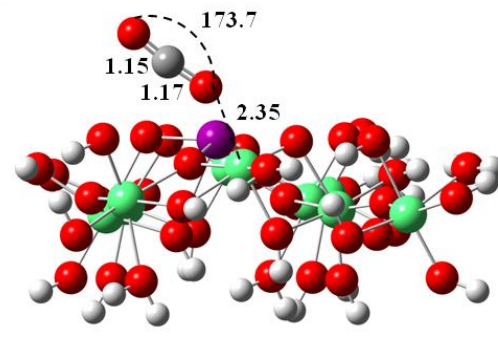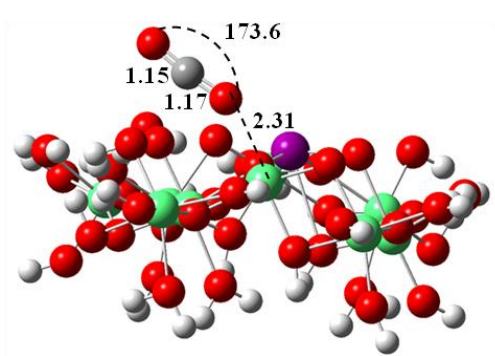
Figure 17: Optimized geometry configurations of CO_2 adsorbed onto the neutral I-doped brookite (210) surface cluster. Colors represent atoms accordingly: Ti in green, O in red, H in white, C in gray, and I in purple. Distances and angles are in Å and degrees, respectively. Configuration 17C has two images presented for better viewing; a front view, 17C(a), and a side view, 17C(b).

18A

18D

18B

18E

18F
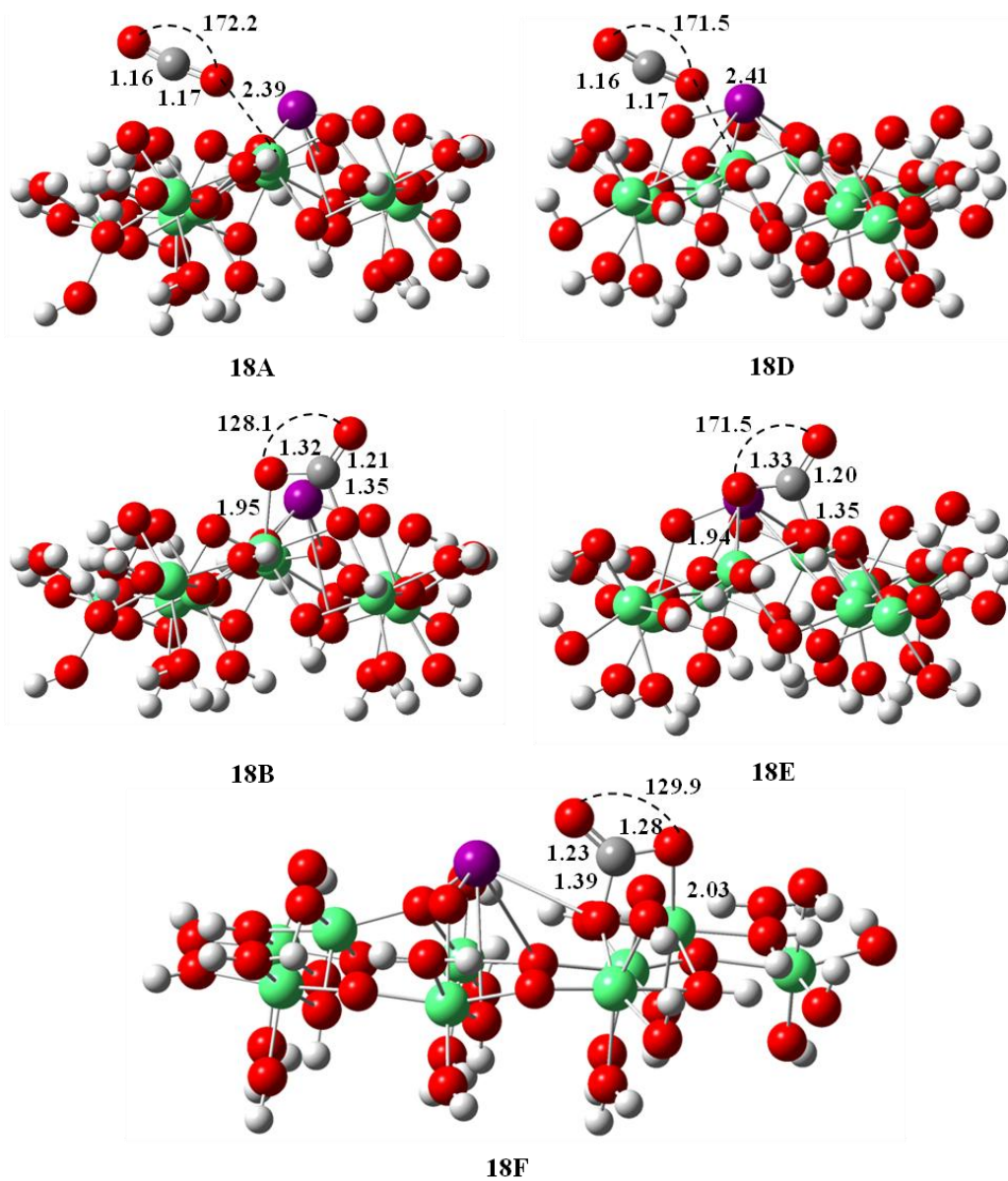
Figure 18: Optimized geometry configurations of CO_2 adsorbed onto the negatively-charged I- doped brookite (210) surface cluster. Colors represent atoms accordingly: Ti in green, O in red, H in white, C in gray, and I in purple. Distances and angles are in Å and degrees, respectively.

Table 5: Calculated Adsorption Energies (in eV) of CO_2 on the Neutral and Negatively-Charged I-doped Anatase (101) and I-doped Brookite (210) Surfaces.

Phase		I-Doped Anatase (101)		I-Doped Brookite (210)	
State		Neutral (Configuration 15)	Negatively-Charged (Configuration 16)	Neutral (Configuration 17)	Negatively-Charged (Configuration 18)
A		-0.22	-0.23	-0.38	-0.34
B		0.00	-0.34	-0.23	-0.54
C		0.53	-0.05	0.50	--[a]
D		--[a]	-0.21	-0.27	-0.24
E		--[a]	-0.27	-0.08	-0.56
F		--[a]	--[a]	--[a]	-0.02

[a] The dashed lines indicate structures converged to already optimized configurations.

The calculated adsorption energies (in eV) of CO_2 bound to the neutral and negatively-charged I-doped anatase as well as the neutral and negatively-charged I-doped brookite surfaces are reported in Table 5.

From Figures 15 and 16 it can be seen that CO_2 interacts with both the neutral and negatively-charged I-doped anatase (101) surface in similar binding configurations. This is also true for the neutral (Figure 17) and negatively-charged (Figures 18) I-doped brookite (210) surface.

On the neutral I-doped anatase surface, three distinct CO_2 configurations exist; configurations 15A, 15B, and 15C. The adsorption energies of the three are -0.22, 0.00, and 0.53 eV, respectively. Of the three, 15A has the lowest adsorption energy making it the most favorable and 15C the most unfavorable. It can be inferred that on the neutral I-doped anatase surface, CO_2 is most likely to bind in an almost linear fashion.

On the negatively-charged I-doped anatase surface, configuration 16B is the most energetically favorable with an adsorption energy of -0.34 eV. Despite being the most energetically favorable, the energy difference between 16B and 16E is insignificant, meaning they are energetically similar. Configurations 16A, 16D, and 16E are energetically equivalent to each other. It should be emphasized that while 16B is energetically similar to 16E, it is not energetically similar to 16A or 16D. Configuration 16C is the most unfavorable of the five configurations, having an adsorption energy of -0.05 eV.

Regarding both neutral and negatively-charged I-doped anatase systems, the negatively-charged surface appears to be the more reactive. Configuration

54

16A and the two additional binding sites (configuration 16D and 16E) are energetically equivalent with 15A. In addition to two new binding sites, configurations 16B-16C have significantly lower adsorption energies to their neutral counterparts (configurations 15B and 15C).

Of the five configurations on the neutral I-doped brookite surface, configuration 17A is the most favorable, experiencing the strongest adsorption energy (-0.38 eV). The adsorption energy of configuration 17B (-0.23 eV) and 17D (-0.27 eV) are energetically equivalent. While configuration 17C and 17E have the more unfavorable energies, 17C has the highest adsorption energy at 0.50 eV.

On the negatively-charged I-doped brookite surface, all configurations are energetically different with the exception of 18B and 18E. Configuration 18B and 18E have the lowest adsorption energies and are the more energetically favorable of the structures. It is important to emphasize that 18B and 18E are energetically equivalent to each other with similar structural features. Even though 18A and 18D are structurally similar, their adsorption energies are significantly different. This same observation was also noticed for configuration 17A and 17D (the neutral I-doped brookite surface). Unlike on the neutral I-doped surface, CO_2 binding to the #1-Ti atom in a similar fashion to 17C doesn't occur. However, CO_2 does bind on the #2-Ti atom in a similar manner to 17C and is labeled 18F. Configuration 18F was the least favorable with an adsorption energy of -0.02 eV.

Concerning the neutral and negatively-charged I-doped brookite surfaces, as was noticed on the I-doped anatase surface, the negatively-charged I-doped brookite surface is more reactive. Unlike on the neutral I-doped brookite surface, all configurations had negative adsorption energies. Configurations 18A and 18D were energetically competitive with their neutral counterparts (configuration 17A and 17D). Configurations 18B and 18E were not only significantly more favorable than their neutral counterparts, but were the most significantly favorable of both neutral and negatively-charged I-doped brookite surfaces.

When considering both the I-doped anatase and I-doped brookite systems as a whole, CO_2 is more likely to adsorb onto the I-doped brookite surface. The neutral I-doped brookite surface has five possible configurations, four of which have negative adsorption energies, as compared to the three configurations on the neutral I-doped anatase surface, of which two have highly unfavorable adsorption energies. The most energetically unfavorable configuration on the neutral I-doped brookite surface (17C) is structurally similar and energetically on par with the neutral I-doped anatase counterpart (15C). While the negatively-charged I-doped anatase surface is an improvement to its neutral surface, the negatively-charged I-doped brookite surface still has significantly more favorable adsorption energies. Configurations 18A, 18B, and 18E are all significantly more stable than their corresponding negatively-charged I-doped anatase configurations.

Charge and Spin Density Analyses of CO$_2$ Adsorbed on the I-Doped Anatase

(101) and I-Doped Brookite (210) Surfaces

Table 6 reports the charge and spin densities of CO$_2$ on the different

configurations for the neutral and negatively-charged I-doped anatase and I-doped

brookite surfaces. The charge values are the sum of the NBO atomic charges on

the CO$_2$ molecule.

On the neutral and negatively-charged I-doped anatase surfaces, negative

charges are located on the CO$_2$ molecule of configurations 15B, 15C, 16B, 16C,

and 16E. These charges are fairly comparable to one another, and are comparable

to their corresponding I-doped brookite counterparts. The CO$_2$ on the I-doped

brookite surface has negative charges for configurations 17B, 17C, 17E, 18B,

18E, and 18F. The spin density was calculated to determine if an unpaired

electron was transferred to the CO$_2$ molecule. The results of the spin density

analysis shows negligible spin on CO$_2$ for both the I-doped anatase and I-doped

brookite surfaces, suggesting no CO$_2^-$ formation. As was seen on the perfect

brookite surface, there is an uneven charge distribution. For all configurations,

the iodine atom retains most of the unpaired electron, refusing to share with CO$_2$.

An example of this uneven distribution is seen in Figure 19. However, since the

overall adsorption energies of the CO$_2$ molecule on the I-doped brookite surface

are lower and the charge transfer is comparable to I-doped anatase, the results

suggest that CO$_2$ will more readily interact with the I-doped brookite (210)

surface than the I-doped anatase (101) surface.

Table 6: Charge and Spin Distributions of CO_2 on the Neutral and Negatively-Charged I-doped Anatase

(101) and I-doped Brookite (210) Surfaces.

Phase	I-Doped Anatase (101)			I-Doped Brookite (210)		
State	Neutral (Configuration 15)		Negatively-Charged (Configuration 16)	Neutral (Configuration 17)		Negatively-Charged (Configuration 18)
	Charge	Spin	Charge	Charge	Spin	Charge
A	0.11	0.00	0.08	0.16	0.00	0.13
B	-0.18	0.00	-0.24	-0.17	0.00	-0.23
C	-0.18	0.01	-0.24	-0.14	0.01	--[a]
D	--[a]	--[a]	0.06	0.14	0.00	0.11
E	--[a]	--[a]	-0.24	-0.16	0.00	-0.24
F	--[a]	--[a]	--[a]	--[a]	--[a]	-0.22

[a] The dashed lines indicate structures that converged to already optimized configurations.

58
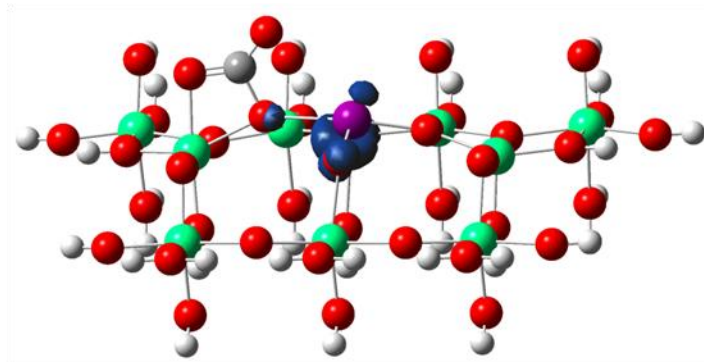
19A
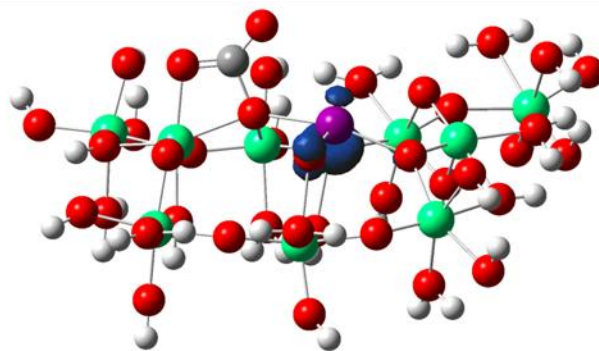
19B

Figure 19: Spin densities of configuration 15C(a) for the neutral anatase (101) TiO_2 surface (19A) and 17C(a) for the brookite (210) TiO_2 surface (19B). Colors represent atoms accordingly: Ti in green, O in red, H in white, C in gray and I in purple. Blue represents unpaired electron.

Comparisons to Perfect TiO_2 Surfaces

Configurations of CO_2 interacting on the I-doped anatase and I-doped brookite surfaces are comparable to the perfect anatase and brookite surfaces, respectively. In both anatase and brookite systems, I-doped and perfect with the

exception of configuration F on the negatively-charged anatase surface, charge and spin density analysis was insignificant.

In the I-doped anatase system, configuration 16B is energetically equivalent to the neutral anatase surface configurations A and B as well as their negatively-charged anatase surface configuration counterparts. Configuration 16E is also energetically equivalent to configuration A of the neutral anatase surface and A and C of the negatively-charged anatase surface. Additionally, all configurations on the negatively-charged I-doped anatase surface are more favorable than the remaining configurations on the anatase surface (E of the neutral anatase surface and E and F of the negatively-charged anatase surface.) The results of the calculations implicate that the negatively-charged I-doped anatase may be equally as reactive as perfect anatase.

Regarding the I-doped brookite surface, it produces several configurations that are energetically comparable to configurations on the perfect brookite surface. Configuration 17A has a similar adsorption energy to configurations 7A, 7C, 8A and 8B. Configurations 17B and 17D are also comparable to 7C. On the negatively-charged I-doped brookite surface, configuration 18A is energetically equivalent to 7C, 8A and 8B. Additionally, configurations 18B and 18E are energetically similar to 7B and 8C. Although the perfect brookite has two configurations (7D and 8D) that are significantly more favorable than any configuration on the I-doped brookite, the I-doped brookite still provides reactivity sites that are on par with perfect brookite reactivity sites.

According to the adsorption energies, CO_2 interaction on the I-doped brookite surface appears to be more favorable than on the perfect anatase surface. CO_2 configurations on the neutral I-doped brookite are comparable to configurations in both the neutral and negatively-charged systems of anatase. The negatively-charged I-doped brookite system has configurations that are energetically equivalent and favorable to the neutral and negatively-charged anatase surface. Neutral I-doped brookite surface configuration 17A is equivalent to the neutral anatase surface configurations A and C. Configuration 17D is comparable to A as well. In the negatively-charged I-doped brookite system, configuration 18A is comparable to the negatively-charged anatase surface configurations A and C. Configuration 18A is also comparable to A and C of the neutral anatase surface. In fact, all configurations on the negatively-charged I-doped brookite surface are more favorable than the neutral configuration E and the negatively-charged configurations E and F of the anatase surface. The important configurations are 18B and 18E, which are comparable to each other, because they have adsorption energies that are significantly more favorable than any of adsorption energies reported for configurations on both the neutral and negatively-charged anatase surface. This suggests that CO_2 is more likely to interact with I-doped brookite than perfect anatase.

Comparisons to Experiments

Little research has been published regarding the photoreduction of CO_2 on I-doped TiO_2. The computational work performed on I-doped TiO_2 suggests that

CO$_2$ will more likely interact with I-doped brookite than perfect anatase or I-doped anatase. Of the published experimental work, the photocatalysts used are mixed-phase TiO$_2$ (Zhang *et al.* 2011; Zhang *et al.* 2012). The primary phases present in the mixture being anatase (major) and brookite (minor) TiO$_2$. Both investigations demonstrated that TiO$_2$ doped iodine have higher photocatalytic activity and more product formation under visible light and UV irradiation than undoped anatase-brookite mixed TiO$_2$ catalyst.

A comparison between the computational work and the experimental work cannot be made directly since the experimental work used a mixed-phase TiO$_2$ catalyst and the computational work looked at pure phase TiO$_2$ clusters at specific surface planes. However, it is clear that both the computational and experimental studies demonstrated that I-doping promotes CO$_2$ interaction on the TiO$_2$ surface. I-doped brookite, from the computational work, was shown to have comparable and more favorable CO$_2$ adsorption energies than perfect brookite and perfect anatase, respectively. The mixed-phase TiO$_2$ with iodine doping from the experimental work was shown to be more photocatalytically active in the photoreduction of CO$_2$than undoped TiO$_2$.   It would be fascinating to see how I-doped pure phase TiO$_2$ catalysts affect CO$_2$ reduction in experimental work. A more direct comparison could then be made between this I-doped computational work and experimental work on pure phase anatase and brookite TiO$_2$ catalyst doped with iodine and their impact on CO$_2$.

Chapter 4

CONCLUSION AND FUTURE WORK

Conclusion

Adsorption energy and charge analysis calculations were performed on the interactions of CO_2 with perfect, oxygen-deficient, and iodine-doped clusters of brookite TiO_2. The intention of this research was to investigate whether the brookite (210) surface had a similar or greater ability as compared to anatase for attracting CO_2 and transferring charge to the CO_2 molecule, thus facilitating the first step in the CO_2 reduction reaction. As demonstrated by previous DFT calculations with other molecules (Li *et al.* 2008), the brookite (210) surface exhibited stronger adsorption of CO_2 in certain configurations. However, unlike on the negatively-charged anatase (101) surface, the CO_2 anion did not form on the negatively-charged brookite (210) surface. Although some of the CO_2 – brookite (210) configurations had more favorable adsorption energetics as compared to the CO_2 interactions with the anatase (101) surface, the computational results suggest that an unmodified brookite (210) surface by itself does not result in charge transfer to the CO_2. However, the presence of oxygen vacancies within the brookite (210) surface enhanced the interaction of CO_2 with the surface and facilitated charge transfer to the CO_2 molecule. The computational data are corroborated with experimental results.

CO$_2$ interacting on iodine-doped surfaces displayed no signs of CO$_2^-$ formation as was demonstrated by little charge transfer to CO$_2$ in both the anatase and brookite systems. Spin density analysis revealed that the insignificant charge transfer to CO$_2$ was the result of the iodine atom retaining most of the charge. However, the adsorption energies were more favorable on I-doped brookite compared to I-doped anatase, suggesting that CO$_2$ has a stronger interaction with I-doped brookite as opposed to I-doped anatase.

The viability of brookite as a potential photocatalyst, particularly oxygen-deficient brookite, for the photocatalytic reduction of CO$_2$ was demonstrated. Ultimately the results that were obtained serve to elucidate the initial step in the overall CO$_2$ photoreduction process, and help to improve the synthesis of a new class of materials for the generation of fuels using the brookite phase of TiO$_2$. The overall purpose behind the research was to make steps toward creating a photocatalyst capable of efficiently converting CO$_2$ to fuels using visible light from the sun as its main source of energy. However, as outlined subsequently, a significant amount of additional work is still required to fully elucidate the CO$_2$ photoreduction mechanism.

Future Work

First-principle calculations were performed on modified and umodified anatase and brookite cluster systems. The purpose was to determine the CO$_2$ interaction on the different surfaces. The results suggest that oxygen-deficient and iodine-doped brookite are more suitable over oxygen-deficient and I-doped

64

anatase, respectively, for CO_2 adsorption and may possibly be suitable photocatalysts for CO_2 reduction. Both perfect and iodine-doped brookite lacked significant charge transfer due to an uneven distribution of charge, in which the Ti and I atom retained most of the charge, respectively. Because it was demonstrated that an oxygen vacancy in brookite improved CO_2 adsorption compared to perfect brookite and facilitated charge transfer with signs of CO_2^- formation, the next step will be to determine the effects on the interaction of CO_2 with anatase and brookite surfaces co-modified with oxygen vacancies and iodine doping. A potential exists for increasing the charge transfer and favorability of CO_2 adsorption to the TiO_2 surfaces. Much larger model surfaces will be needed to examine the effects of oxygen vacancies and iodine co-modifications.

Another area of interest is the effect of metal (such as copper) and iodine co-modifications to a larger TiO_2 model. Experimental work was performed on the photocatalytic reduction of CO_2 using copper and iodine co-modified TiO_2 (Zhang *et al.* 2012). Carbon monoxide (CO) was the major product with trace amounts of methane (CH_4) and methyl chloride (CH_3Cl). The results demonstrated that copper and iodine co-modified TiO_2 increased CO_2 photoreduction under UV-vis and visible light irradiation compared to pure TiO_2. It was determined that iodine doping promoted visible light activity and copper species facilitated charge transfer and increased the photoreduction of CO_2. A mechanism in which CO_2 is first reduced to CO through a two-electron and two-proton reaction was suggested. However, further study is necessary to validate

this mechanism. Computational work can provide further insight on what may be occurring between CO_2 and the photocatalyst's surface.

Lastly, a full examination of the product formation mechanism in the CO_2 photoreduction process from a computational perspective would be highly valuable. This computational aspect would provide insight into the possible transition states of CO_2 photoreduction and the type of product each possible state leads to. Essentially, an energy diagram can be created to model the different possible product pathways. If these pathways can be understood, further work can be devoted to improving photocatalytic materials suited to specific product formations.

REFERENCES

Addamo, M., M. Bellardita, A. Di Paola, and L. Palmisano. 2006. Preparation and photoactivity of nanostructured anatase, rutile and brookite TiO_2 thin films. *Chemical Communications* (47):4943-4945.

Agrios, A. G., K. A. Gray, and E. Weitz. 2003. Photocatalytic transformation of 2,4,5-trichlorophenol on TiO_2 under sub-band-gap illumination. *Langmuir* 19 (4):1402-1409.

Anpo, M., H. Yamashita, Y. Ichihashi, and S. Ehara. 1995. Photocatalytic reduction of CO_2 with H_2O on various Titanium-Oxide catalysts. *Journal of Electroanalytical Chemistry* 396 (1-2):21-26.

Aschauer, U., Y.B. He, H.Z. Cheng, S.C. Li, U. Diebold, and A. Selloni. 2010. Influence of subsurface defects on the surface reactivity of TiO_2: Water on anatase (101). *Journal of Physical Chemistry C* 114(2):1278-1284.

Bagwasi, S., B. Z. Tian, F. Chen, and J. L. Zhang. 2012. Synthesis, characterization and application of iodine modified titanium dioxide in phototcatalytical reactions under visible light irradiation. *Applied Surface Science* 258 (8):3927-3935.

Becke, A. D., J. 1993. Density-functional thermochemistry. III. The role of exact exchange. *Journal of Chemical Physics* 98:5648-5652.

Belelli, P.G., R.M. Ferullo, M.M. Branda, and N.J. Castellani, Theoretical modeling of photocatalytic active species on illuminated TiO2. *Applied Surface Science*. 254(1):32-35.

Bruska, M.K., K. Szacilowski, and J. Piechota. 2009. Adsorption of selected ions on the anatase TiO2 (101) surface: A density-functional study. Molecular *Simulation* 35(7):567-576.

Centi, G., and S. Perathoner. 2009. Opportunities and prospects in the chemical recycling of carbon dioxide to fuels. *Catalysis Today* 148 (3-4):191-205.

Chai, J. W., M. Yang, Q. Chen, J. S. Pan, Z. Zhang, Y. P. Feng, and S. J. Wang. 2011. Effects of nitrogen incorporation on the electronic structure of rutile-TiO_2. *Journal of Applied Physics* 109 (2):4.

Clark, T., J. Chandrasekhar, G. W. Spitznagel, and P. V. R Schleyer. 1983. Efficient diffuse function-augmented basis-sets for anion calculations. 3. The 3-21+G basis set for 1st-row elements, Li-F. *Computational Chemistry* 4:294-301.

Cramer, C.J. and D.G. Truhlar. 2009. Density functional theory for transition metals and transition metal chemistry. PCCP. 11(46):10757-10816.

Dambournet, D., I. Belharouak, and K. Amine. 2010. Tailored preparation methods of TiO_2 anatase, rutile, brookite: Mechanism of formation and electrochemical properties. *Chemistry of Materials* 22 (3):1173-1179.

Deskins, N. A., R. Rousseau, and M. Dupuis. 2010. Defining the Role of Excess Electrons in the Surface Chemistry of TiO_2. *Journal of Physical Chemistry C* 114 (13):5891-5897.

Di Paola, A., G. Cufalo, M. Addamo, M. B. Ellardita, R. Campostrini, M. Ischia, R. Ceccato, and L. Palmisano. 2008. Photocatalytic activity of nanocrystalline TiO_2 (brookite, rutile and brookite-based) powders prepared by thermohydrolysis of $TiCl_4$ in aqueous chloride solutions. *Colloids and Surfaces a-Physicochemical and Engineering Aspects* 317 (1-3):366-376.

Diebold, U., N. Ruzycki, G.S. Herman, and A. Selloni. 2003. One step towards bridging the materials gap: surface studies of TiO_2 anatase. *Catalysis Today* 85(2-4):93-100.

Ditchfield, R., W. J. Hehre, and J.A. Pople. 1971. Self-Consistent Molecular Orbital Methods. 9. Extended Gaussian-type basis for molecular-orbital studies of organic molecules. *Journal of Chemical Physics* 54:724.

Finazzi, E., C. Di Valentin, G. Pacchioni, and A. Selloni. 2008. Excess electron states in reduced bulk anatase TiO2: Comparison of standard GGA, GGA plus U, and hybrid DFT calculations. *Journal of Physical Chemistry* 129(15):154113.

Frisch, M. J., J. A. Pople, and J. S. Binkley. 1984. Self-Consistent Molecular Orbital Methods. 25. Supplementary Functions for Gaussian Basis Sets. *Journal of Chemical Physics* 80:3265-3269.

Frisch, M. J.; G.W. Trucks, H. B. Schlegel, G. E. Scuseria, M. A. Robb, J. R. Cheeseman, J. A. Jr Montgomery, T. Vreven, K. N. Kudin, J. C. Burant, J. M. Millam, S. S. Iyengar, J. Tomasi, V. Barone, B. Mennucci, M. Cossi, G. Scalmani, N. Rega, G. A. Petersson, H. Nakatsuji, M. Hada, M. Ehara, K. Toyota, R. Fukuda, J. Hasegawa, M. Ishida, T. Nakajima, Y. Honda, O. Kitao, H. Nakai, M. Klene, X. Li, J. E. Knox, H. P. Hratchian, J. B. Cross, V. Bakken, C. Adamo, J. Jaramillo, R. Gomperts, R. E. Stratmann, O. Yazyev, A. J. Austin, R. Cammi, C. Pomelli, J. W. Ochterski, P. Y. Ayala, K. Morokuma, G. A. Voth, P. Salvador, J. J. Dannenberg, V. G. Zakrzewski, S. Dapprich, A. D. Daniels, M. C. Strain, O. Farkas, D. K. Malick, A. D. Rabuck, K. Raghavachari, J. B. Foresman, J. V. Ortiz, Q. Cui, A. G. Baboul, S. Clifford, J. Cioslowski, B. B. Stefanov, G. Liu, A.

Liashenko, P. Piskorz, I. Komaromi, R. L. Martin, D. J. Fox, T. Keith, M. A. Al-Laham, C. Y. Peng, A. Nanayakkara, A., M. Challacombe, P. M. Gill, B. Johnson, W. Chen, M. W. Wong, C. Gonzalez, and J. A. Pople. Gaussian 03; Gaussian, Inc.: Wallingford, CT, 2004.

Gong, X. Q., and A. Selloni. 2007. First-principles study of the structures and energetics of stoichiometric brookite TiO_2 surfaces. *Physical Review B* 76 (23).

Hamadanian, M., A. Reisi-Vanani, and A. Majedi. 2009. Preparation and characterization of S-doped TiO_2 nanoparticles, effect of calcination temperature and evaluation of photocatalytic activity. *Materials Chemistry and Physics* 116 (2-3):376-382.

Hay, P. J. and W. R. Wadt. 1985. Ab initio effective core potentials for molecular calculations - potentials for the transition-metal atoms Sc to Hg. *Journal of Chemical Physics* 82:270-283.

Hay, P. J. and W. R. Wadt. 1985. Ab initio effective core potentials for molecular calculations - potentials for K to Au including the outermost core orbitals. Journal of Chemical Physics 82:299-310.

He, H. Y., P. Zapol, and L. A. Curtiss. 2010. A theoretical study of CO_2 anions on anatase (101) surface. *Journal of Physical Chemistry C* 114 (49):21474-21481.

Hehre, W. J., R. Ditchfield, and J. A. Pople. 1972. Self-Consistent Molecular Orbital Methods. 12. Further extensions of Gaussian-type basis sets for use in molecular-orbital studies of organic-molecules. *Journal of Chemical Physics* 56: 2257.

Henderson, M. A. 1998. Evidence for bicarbonate formation on vacuum annealed TiO_2(110) resulting from a precursor-mediated interaction between CO_2 and H_2O. *Surface Science* 400 (1-3):203-219.

Henderson, M. A. 2011. A surface science perspective on TiO_2 photocatalysis. *Surface Science Reports* no. 66 (6-7):185-297.

Homann, T., T. Bredow, and K. Jug. 2004. Adsorption of small molecules on the anatase(100) surface. *Surface Science* 555(1-3):135-144.

Hong, X. T., Z. P. Wang, W. M. Cai, F. Lu, J. Zhang, Y. Z. Yang, N. Ma, and Y. J. Liu. 2005. Visible-light-activated nanoparticle photocatalyst of iodine-doped titanium dioxide. *Chemistry of Materials* 17 (6):1548-1552.

Hurum, D. C., A. G. Agrios, S. E. Crist, K. A. Gray, T. Rajh, and M. C. Thurnauer. 2006. "Probing reaction mechanisms in mixed phase TiO2 by

EPR." *Journal of Electron Spectroscopy and Related Phenomena* 150 (2-3):155-163.

Hurum, D. C., A. G. Agrios, K. A. Gray, T. Rajh, and M. C. Thurnauer. 2003. Explaining the enhanced photocatalytic activity of Degussa P25 mixed-phase TiO_2 using EPR. *Journal of Physical Chemistry B* 107 (19):4545-4549.

Indrakanti, V. P., J. D. Kubicki, and H. H. Schobert. 2008. Quantum chemical modeling of ground states of CO_2 chemisorbed on anatase (001), (101), and (010) TiO_2 surfaces." *Energy & Fuels* 22 (4):2611-2618.

Indrakanti, V.P., H.H. Schobert, and J.D. Kubicki. 2009. Quantum mechanical modeling of CO_2 interactions with irradiated stoichiometric and oxygen-deficient anatase TiO_2 surfaces: Implications for the photocatalytic reduction of CO_2. Energy & Fuels 23:5247-5256.

Indrakanti, V. P., J. D. Kubicki, and H. H. Schobert. 2009. "Photoinduced activation of CO_2 on Ti-based heterogeneous catalysts: Current state, chemical physics-based insights and outlook." *Energy & Environmental Science* 2 (7):745-758.

Kandiel, T. A., A. Feldhoff, L. Robben, R. Dillert, and D. W. Bahnemann. 2010. Tailored titanium dioxide nanomaterials: anatase nanoparticles and brookite nanorods as highly active photocatalysts. *Chemistry of Materials* 22 (6):2050-2060.

Kitano, M., M. Matsuoka, M. Ueshima, and M. Anpo. 2007. Recent developments in titanium oxide-based photocatalysts. *Applied Catalysis A-General* 325 (1):1-14.

Koci, K., K. Mateju, L. Obalova, S. Krejcikova, Z. Lacny, D. Placha, L. Capek, A. Hospodkova, and O. Solcova. 2010. Effect of silver doping on the TiO_2 for photocatalytic reduction of CO_2. *Applied Catalysis B-Environmental* 96 (3-4):239-244.

Koci, K., L. Obalova, and Z. Lacny. 2008. Photocatalytic reduction of CO_2 over TiO_2 based catalysts. *Chemical Papers* 62 (1):1-9.

Koelsch, M., S. Cassaignon, J. F. Guillemoles, and J. R. Jolivet. 2002. Comparison of optical and electrochemical properties of anatase and brookite TiO_2 synthesized by the sol-gel method. *Thin Solid Films* 403:312-319.

Labat, F., P. Baranek, C. Domain, C. Minot, and C. Adamo. 2007. Density functional theory analysis of the structural and electronic properties of

TiO2 rutile and anatase polytypes: Performances of different exchange-correlation functionals. *Journal of Physical Chemistry* 126(15):154703.

Lazzeri, M., A. Vittadini, and A. Selloni. 2001. Structure and energetics of stoichiometric TiO2 anatase surfaces. *Physical Review B* 6315(15):155409.

Lee, C. T., W.T. Yang, and R.G. Parr. 1988. Development of the Colle-Salvettii correlation-energy formula into a functional of the electron density. *Physical Review B* 37:785-789.

Li, J. G., T. Ishigaki, and X. D. Sun. 2007. Anatase, brookite, and rutile nanocrystals via redox reactions under mild hydrothermal conditions: Phase-selective synthesis and physicochemical properties. *Journal of Physical Chemistry C* 111 (13):4969-4976.

Li, L., H. S. Zhuang, and D. Bu. 2011. Characterization and activity of visible-light-driven TiO2 photocatalyst codoped with lanthanum and iodine. *Applied Surface Science* 257 (21):9221-9225.

Li, W. K., X. Q. Gong, G. Lu, and A. Selloni. 2008. Different reactivities of TiO_2 polymorphs: Comparative DFT calculations of water and formic acid adsorption at anatase and brookite TiO_2 surfaces. *Journal of Physical Chemistry C* 112 (17):6594-6596.

Li, Y., W. N. Wang, Z. L. Zhan, M. H. Woo, C. Y. Wu, and P. Biswas. 2010. Photocatalytic reduction of CO_2 with H_2O on mesoporous silica supported Cu/TiO_2 catalysts. *Applied Catalysis B-Environmental* 100 (1-2):386-392.

Linsebigler, A. L., G. Q. Lu, and J. T. Yates. 1995. Photocatlysis on TiO_2 surfaces – principles, mechanisms, and selected results. *Chemical Reviews* 95 (3):735-758.

Long, R., Y. Dai, and B. B. Huang. 2009. Structural and electronic properties of iodine-doped anatase and rutile TiO_2. *Computational Materials Science* 45 (2):223-228.

Lopez, R., R. Gomez, and M. E. Llanos. 2009. Photophysical and photocatalytic properties of nanosized copper-doped titania sol-gel catalysts. *Catalysis Today* 148 (1-2):103-108.

Merrick, J. P., D. Moran, and L. Radom. 2007. An evaluation of harmonic vibrational frequency scale factors. *Journal of Physical Chemistry A* 111 (45):11683-11700.

Pacchioni, G. 2008. Modeling doped and defective oxides in catalysis with density functional theory methods: Room for improvements. Journal of Chemical Physics 128(18):182505.

Pan, H., B. H. Gu, and Z. Y. Zhang. 2009. Phase-dependent photocatalytic ability of TiO_2: A first-principles study. *Journal of Chemical Theory and Computation* 5 (11):3074-3078.

Park, J. Y., C. Lee, K. W. Jung, and D. Jung. 2009. Structure related photocatalytic properties of TiO_2. *Bulletin of the Korean Chemical Society* 30 (2):402-404.

Pelaez, Miguel, Armah A. de la Cruz, Elias Stathatos, Polycarpos Falaras, and Dionysios D. Dionysiou. 2009. Visible light-activated N-F-codoped TiO_2 nanoparticles for the photocatalytic degradation of microcystin-LR in water. *Catalysis Today* 144 (1-2):19-25.

Ramis, G., G. Busca, and V. Lorenzelli. 1991. Low-temperature CO_2 adsorption on metal-oxides – Spectroscopic characterization of some weakly adsorbed species. *Materials Chemistry and Physics* 29 (1-4):425-435.

Rasko, J., and F. Solymosi. 1994. Infrared spectroscopic study of the photoinduced activation of CO_2 on TiO_2 and Rh/TiO_2 catalysts. *Journal of Physical Chemistry* 98 (29):7147-7152.

Scaranto, J. and S. Giorgianni. 2009. A DFT study of CO adsorbed on clean and hydroxylated anatase TiO_2 (001) surfaces. *Molecular Physics* 107(19):1997-2003.

Song, K. Y., Y. T. Kwon, G. J. Choi, and W. I. Lee. 1999. Photocatalytic activity of Cu/TiO_2 with oxidation state of surface-loaded copper. *Bulletin of the Korean Chemical Society* 20 (8):957-960.

Su, W., Y. Zhang, Z. Li, L. Wu, X. Wang, J. Li, and X. Fu. 2008. Multivalency iodine doped TiO_2: Preparation, characterization, theoretical studies, and visible-light photocatalysis. *Langmuir* 24 (7):3422-3428.

Su, W. G., J. Zhang, Z. C. Feng, T. Chen, P. L. Ying, and C. Li. 2008. Surface phases of TiO_2 nanoparticles studied by UV Raman spectroscopy and FT-IR spectroscopy. *Journal of Physical Chemistry C* 112 (20):7710-7716.

Tseng, I. H., and J. C. S. Wu. 2004. Chemical states of metal-loaded titania in the photoreduction of CO_2. *Catalysis Today* 97 (2-3):113-119.

Usubharatana, P., D. McMartin, A. Veawab, and P. Tontiwachwuthikul. 2006. Photocatalytic process for CO_2 emission reduction from industrial flue gas streams. *Industrial & Engineering Chemistry Research* 45 (8):2558-2568.

Varghese, O. K., M. Paulose, T. J. LaTempa, and C. A. Grimes. 2009. High-rate solar photocatalytic conversion of CO_2 and water vapor to hydrocarbon fuels. *Nano Letters* 9 (2):731-737.

Vittadini, A., M. Casarin, and A. Selloni. 2007. Chemistry of and on TiO2-anatase surfaces by DFT calculations: a partial review. *Theoretical Chemistry Accounts* 117(5-6): 663-671.

Wadt, W. R. and P. J Hay. 1985. Ab initio effective core potentials for molecular calculations - potentials for main group elements Na to Bi. Journal of Chemical Physics 82:284-298.

Wen, C., L. Sun, J. M. Zhang, H. Deng, and P. Wang. 2006. Effect of iodine-doping on photocatalytic activity of TiO_2 photocatalyst. *Chemical Journal of Chinese Universities-Chinese* 27 (12):2408-2410.

Wen, Chen, Yu-Jie Zhu, Takaki Kanbara, Hua-Zhang Zhu, and Chang-Fa Xiao. 2009. Effects of I and F codoped TiO_2 on the photocatalytic degradation of methylene blue. *Desalination* 249 (2):621-625.

White, C. M., B. R. Strazisar, E. J. Granite, J. S. Hoffman, and H. W. Pennline. 2003. Separation and capture of CO_2 from large stationary sources and sequestration in geological formations - Coalbeds and deep saline aquifers. *Journal of the Air & Waste Management Association* 53 (6):645-715.

Xie, J. M., X. M. Lu, J. Liu, and H. M. Shu. 2009. Brookite titania photocatalytic nanomaterials: Synthesis, properties, and applications. *Pure and Applied Chemistry* 81 (12):2407-2415.

Yang, C. C., Y. H. Yu, B. van der Linden, J. C. S. Wu, and G. Mul. 2010. Artificial photosynthesis over crystalline TiO_2-based catalysts: Fact or fiction?. *Journal of the American Chemical Society* 132 (24):8398-8406.

Yang, H. C., H. Y. Lin, Y. S. Chien, J. C. S. Wu, and H. H. Wu. 2009. Mesoporous TiO_2/SBA-15, and Cu/TiO_2/SBA-15 bomposite photocatalysts for photoreduction of CO_2 to methanol. *Catalysis Letters* 131 (3-4):381-387.

Zhang, Q. Y., Y. Li, E. A. Ackerman, M. Gajdardziska-Josifovska, and H. L. Li. 2011. Visible light responsive iodine-doped TiO_2 for photocatalytic reduction of CO_2 to fuels. *Applied Catalysis A-General* 400 (1-2):195-202.

Zhang, Q. Y., T. Gao, J. M. Andino, Y. Li. 2012. Copper and iodine co-modified TiO_2 nanoparticles for improved activity of CO_2 photoreduction with water vapor. *Applied Catalysis B-Environmental* 123-124:257-264.

BIOGRAPHICAL SKETCH

Monique Marie Rodriguez was born in Florence, Arizona on January 24, 1988. She received her elementary education in Casa Grande, Arizona. Her secondary education was completed at Casa Grande Union High School in Casa Grande, Arizona. In 2006, Monique entered Arizona State University, Tempe, Arizona, majoring in Chemical Engineering. She graduated in May 2010 and decided to further her education. In August 2010, she returned to Arizona State University to pursue a Master of Science in Chemical Engineering. She received a two year National Science Foundation – Bridge to the Doctorate Fellowship from 2010 – 2012 to pursue her studies.